INFORMATION TO USERS

This material was produced from a microfilm copy of the original document. While the most advanced technological means to photograph and reproduce this document have been used, the quality is heavily dependent upon the quality of the original submitted.

The following explanation of techniques is provided to help you understand markings or patterns which may appear on this reproduction.

1. The sign or "target" for pages apparently lacking from the document photographed is "Missing Page(s)". If it was possible to obtain the missing page(s) or section, they are spliced into the film along with adjacent pages. This may have necessitated cutting thru an image and duplicating adjacent pages to insure you complete continuity.

2. When an image on the film is obliterated with a large round black mark, it is an indication that the photographer suspected that the copy may have moved during exposure and thus cause a blurred image. You will find a good image of the page in the adjacent frame.

3. When a map, drawing or chart, etc., was part of the material being photographed the photographer followed a definite method in "sectioning" the material. It is customary to begin photoing at the upper left hand corner of a large sheet and to continue photoing from left to right in equal sections with a small overlap. If necessary, sectioning is continued again — beginning below the first row and continuing on until complete.

4. The majority of users indicate that the textual content is of greatest value, however, a somewhat higher quality reproduction could be made from "photographs" if essential to the understanding of the dissertation. Silver prints of "photographs" may be ordered at additional charge by writing the Order Department, giving the catalog number, title, author and specific pages you wish reproduced.

5. PLEASE NOTE: Some pages may have indistinct print. Filmed as received.

Xerox University Microfilms
300 North Zeeb Road
Ann Arbor, Michigan 48106

A model study of the effect of an atmospheric thermal plume on a line-of-sight radio link

by

Vera Onthuam

A Dissertation Submitted to the
Graduate Faculty in Partial Fulfillment of
The Requirements for the Degree of
DOCTOR OF PHILOSOPHY
Major: Electrical Engineering

Approved:

Signature was redacted for privacy.

In Charge of Major Work

Signature was redacted for privacy.

For the Major Department

Signature was redacted for privacy.

For the Graduate College

Iowa State University
Ames, Iowa

1973

TABLE OF CONTENTS

		Page
I.	INTRODUCTION	1
II.	THEORY OF LINE-OF-SIGHT RADIO LINKS	6
III.	THE NATURE OF AN ATMOSPHERIC THERMAL PLUME	8
IV.	THEORY OF OPTICAL SCALING OF THE RADIO LINK	13
V.	EXPERIMENTAL SET UP AND PROCEDURE	21
	V.1. The Set Up	21
	V.2. The Calibration and Testing of the Instruments	26
	V.3. The Experimental Procedure	35
VI.	RESULTS	42
VII.	CONCLUSION	53
VIII.	BIBLIOGRAPHY	56
IX.	ACKNOWLEDGMENT	59
X.	APPENDIX: THEORY OF THE SCHLIEREN SYSTEM	60

I. INTRODUCTION

This dissertation describes an experimental study of the effects of an atmospheric thermal plume on the propagation of electromagnetic waves over a line-of-sight radio link. The objectives of this study are: (1) to determine the feasibility of the use of an optical modeling technique to study atmospheric interactions at radio frequencies and (2) to use the model in evaluating the effect of a thermal plume on line-of-sight radio wave propagation paths.

Electromagnetic waves propagating through the atmosphere suffer a degradation due to the interaction between the waves and the changing atmosphere. These effects include: refraction, scattering, and reflection; which result in multiple propagation paths and a highly variable signal level. This phenomenon is called "fading".

For many years radio physicists and engineeers have studied fading and proposed mechanisms and theories to account for its characteristics. There have been many experiments performed by these scientists and engineers using actual communication links as the propagation path. Many papers have reported signal-level curves, fading frequencies, fading periods, and depth-of-fade measurements for particular paths and specific frequencies. To study other paths, in other locations, the equipment and personnel must be moved to the other sites to record the data for a period of time. A fundamental drawback of this type of experimental method is the expense involved.

A well-known technique, long used by antenna engineers, is the principle of frequency scaling. When designing a large-sized antenna they experienced problems in determining the antenna pattern because of the space required for the measurement of the far field. To get away from this problem, they built another antenna of the same configuration but of smaller size and used a higher frequency in measuring the pattern. Skolnik [1], using the scaling technique, scaled an antenna measuring 38 feet in diameter at 1800 MHz, down to 1.4 feet in diameter at 35 GHz. Redlien and Heinemann [2] have used 0.63 micrometer wavelength laser radiation to simulate a 75 wavelength diameter antenna at X band frequencies (8.2-12.4 GHz). They did not reduce the antenna by the true scaling factor but did get a good qualitative pattern of the antenna. In 1957 Holt and Spencer [3] used a light source and a scaled model of an aircraft to simulate the back scattering of a radar signal from the full sized aircraft. Another experiment, performed by Edison [4] to study the propagation of waves in a random medium, used acoustic waves propagating through artificially generated turbulence in a water tank. By heating the bottom of the tank, convection caused blobs of hot water to rise to the surface, and produced a fluctuation of the signal. Recently, Post, Guidry, and Rost [5] reported on the use of an earth model and a laser to simulate the propagation of an electromagnetic wave over the earth's horizon. They used a pyrex disc with a convex spherical surface as the earth model, and detected the amount of energy reaching the receiver on a photographic

plate. Thus, the way has been opened for us to investigate the possibilities of using optical simulation techniques to study radio wave propagation characteristics on a line-of-sight radio link in the troposphere.

Recent papers on remote sensing of the atmospheric structure [6, 7, 8] by means of an acoustic echo-sounding method have helped resolve features of the temperature and wind field in the lower atmosphere. This method has been helpful in studying thermal or convective plumes. Hall [6] recently reported on the detection of thermal plumes in the atmosphere by this method. He remarked that: (1) the plumes were vigorous on sunny days; (2) wind shear produced a slope sometimes into, and sometimes with the wind; (3) the plume height increased with time starting in the morning and reaching a maximum shortly after noon; and (4) there was very little change in plume characteristics with the season. He also reported that the acoustic echo-sounding observations were consistent with the observation made by Kaimal and Businger [9] using fast response thermometers and anemometers on a tower.

Bean [8] employed an FM-CW radar at 10 cm wavelength and acoustic echo-sounding equipment simultaneously with in-situ measurements of the scattering region and found that the radar reflectivities were in good agreement with the reflectivities computed from the measured data. From his acoustic echo sounder's facsimile record, he found that there were some echoes due to convective plumes in the atmosphere, and he observed that they agree with the convective plume model of Kaimal and Businger.

From these results, it is apparent that the convective thermal plume is a frequently encountered phenomenon in the lower atmosphere. As described by Kaimal and Businger [9], the thermal plume is a thermally generated atmospheric activity. It has a higher internal temperature than the air outside the boundary thus having a different radio refractivity. The boundary, the motion of the air inside boundary, and the mixing and tilting of the structure can be expected to affect radio wave propagation if it is located in the path of the wave. Until now, most of the research in this area has been devoted to the study of the effects of the thermal plume on the back-scattering of the waves such as the returned radar signal and acoustic echo-sounding signal. Very little work has been done on the effects of the thermal plume on the waves scattered in the forward direction. Using the scaling techniques mentioned earlier an experimental investigation can be performed in the laboratory. The implementation of these scaling techniques to study the effect of a thermal plume on the propagation characteristics of a line-of-sight communication path is the subject of this study.

The next part of the dissertation deals with the theory of line-of-sight propagation. A brief explanation of the effects of various meteorological phenomena on radio wave propagation including the effects of a thermal plume is presented. Part III contains a detailed explanation of the atmospheric thermal plume based on its physical structure and behavior as observed by Kaimal and Businger [9]. The theory of

optical scaling of a radio link and the thermal plume is also contained in part IV. Included in this section is a theoretical treatment on the factors to be considered in scaling the natural thermal plume the size of about 100 m in diameter to the size of 1.275 cm.

The detailed explanation of the construction of the set up, and the procedure followed in the performance of the experiment are contained in part V. In this section are shown a photograph and diagrams of the experimental setup and schematics of the electronics circuitry. The results of the experiments are tabulated in part VI. The principle of the Schlieren system, which plays an important role in this experiment, is described in the appendix.

II. THEORY OF LINE-OF-SIGHT RADIO LINKS

The transmission of radio waves over direct line-of-sight paths with nothing in the intervening medium should be such that the received field strength be equal to the theoretical value for propagation over an equivalent free-space path. However in the real-world situation this is not possible because the electromagnetic field at the receiver can be the result of interference between the direct ray and a reflected ray. This interference gives rise to reinforced field strengths when direct and reflected fields are in-phase, and reduced field strengths when they are in phase opposition [10]. Since the refractive index may vary from time-to-time and from point-to-point, the amplitude and phase of the direct and reflected rays at a given point will not be the same from one moment to the next and the regions of strong and weak field strength will shift in space. If the direct and reflected signals are of approximately equal amplitude and in phase opposition, the fading will be severe and the received signal level will be 10 dB or more below the normal theoretical value. There may be instances that the waves bend away from the receiving antenna due to a refracting layer; the fading may be severe in this situation too [11, 12].

If the waves propagate through a small-scale inhomogeneous medium, the received signal will fluctuate with small-amplitude, short-period, variations. This type of fading is sometimes called scintillation of the signal. In between the severe fading and scintillation there are

low amplitude fades due to the effect of medium scale atmospheric phenomena. One objective of this study is to place the atmospheric thermal plume in one or more of these categories.

A narrow beam radio wave propagating through a region where a thermal plume occurs will be affected by the following basic interactions: (1) reflection of wave at the interface of the boundary of the plume and the surrounding air, (2) refraction of wave within the plume boundary, and (3) scattering by the eddies of the plume mixing with outside air. The level of fading may not reach 10 dB below the normal level as often occurs in the case of refracting layer interacting with the beam.

III. THE NATURE OF AN ATMOSPHERIC THERMAL PLUME

During the daylight hours the sun radiates energy through the atmosphere to the surface of the earth in the form of wide-frequency-spectrum electromagnetic waves ranging from invisible ultraviolet wavelengths to the infrared wavelengths. Approximately one-half of the radiated energy is in the visible portion of the spectrum [13]. The maximum radiation is found to be at a wavelength of 4743 Å [14]. This is called short-wave solar radiation. The earth's surface, after absorbing the solar radiation, re-emits at a longer wave length of about 10,000 Å back to the atmosphere. This is called long-wave terrestrial radiation.

Since the earth's surface layer is not homogeneous, all portions of the surface do not absorb the same amount of solar energy. Some areas may be predominantly dry soil, other areas may be wet soil, water or sea, and yet other areas may be covered with vegetation, like the jungles. This difference in absorption causes a difference in the temperature of the surface, even at a separation distance of hundreds of feet. The air directly above the heated surface is warmed to different temperatures at different locations.

From the equation of state: $p\alpha = RT$, where p is the pressure, α is the specific volume ($\alpha = 1/\rho$), R is the specific gas constant and T is the absolute temperature, we see that, at the surface, the parcels of air of differing temperatures will exhibit differences in specific volume or density. That is, the higher the temperature the

the lower the density of the particular parcel of air. Consider a local air parcel in hydrostatic equilibrium before it is heated. The air parcel remains in static equilibrium by the balancing of gravitational and pressure forces; assuming no horizontal movement. Any temperature changes of the parcel, even as small as 1^{o} F, will tip the balance of these forces. The parcel will first expand and then rise upward. The upward acceleration depends on the temperature difference between the air parcel and the surrounding air [15]. The upward air stream, confined into a column of rising air, is called a "thermal" or a "thermal plume" or a "convective plume". This theory assumes that the air in the plume does not mix, or exchange heat with the surrounding air. External to the plume the pressure decreases with increasing height. As the heated air ascends, it will adjust its internal pressure (at sonic speed) to that of the surrounding air. Thus, the pressure of the heated air is equal to the pressure of the surrounding air at all times. The expansion of the plume requires some heat input, and since the heat supplied by the surface ceases shortly after the air parcel leaves the surface, the internal energy of the air parcel is the only source of energy available. The internal energy of a gas is a function of its temperature; thus, as the air parcel moves upward its temperature decreases. If the adiabatic temperature lapse rate is greater than the temperature lapse rate of the surrounding air, the air parcel in the

plume will ascend until its temperature is equal to that of the surrounding air at some height.

There are several papers (Telford [16], Priestley and Ball [17], and Kuo's [18] papers) proposing a theoretical basis for the thermal plume. Most of these papers deal with idealized cases of free convection without wind shear. Recently an experimental program to determine the physical characteristics and the mechanisms that maintain the thermal plume in the earth's atmosphere was conducted by Kaimal and Businger [9]. This is the only paper dealing with instrumental measurements at this time. They reported that, in reality, there is considerable entrainment of air at higher levels above the surface, and that the plume maintains a tilt in the presence of wind shear by means of vertical stretching along the plume. The temperature lapse rate is close to the adiabatic process. From their data, the size of a typical plume is about 60 meters in diameter at the surface and about 40 meters in diameter at the height of 22.6 meters.

Figure 3.1 shows the model of the convective plume given by Kaimal and Businger. The horizontal component of the velocity vector close to the surface is about 2.06 to 2.60 meters per second within the plume boundary. The plume moved slowly with the low-speed surface wind and still retained its identity as a column by stretching.

If the atmosphere is stably stratified, the plume will rise and level off. Bending of the plume is caused by an increase of the horizontal wind velocity. If the horizontal wind shear with height is strong enough, the plume may be broken up and lose its identity. The effect of the

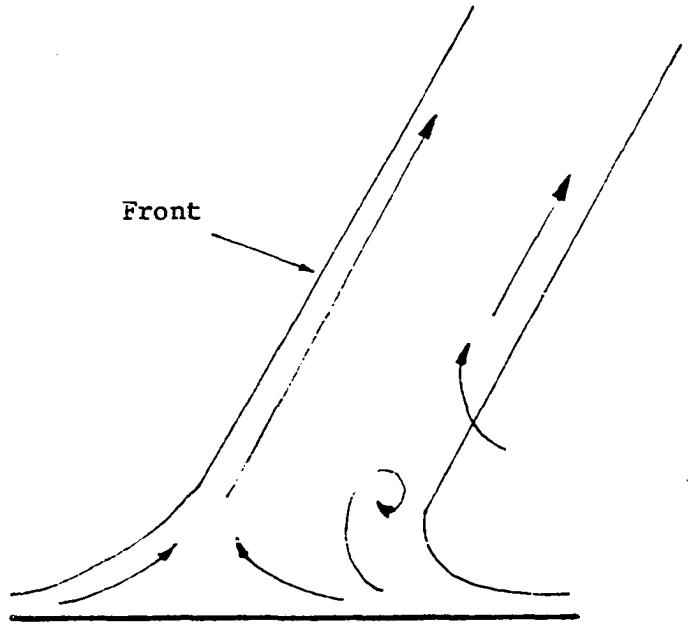

Figure 3.1. The two-dimensional model of the convective plume (after Kaimal and Businger).

wind shear is to introduce vorticity into the flow of the plume. The plume will contain more eddies and the outside air is mixed into the flow boundary not only by entrainment but also by the vorticity of the shear. The result is that it becomes more turbulent and the temperature gradient is more severe. Figure 3.2 (a) and (b) shows the effects of horizontal wind on the thermal plume.

When the thermal plume occurs in the area along the line-of-sight radio link or if one should move past this link, there may be some fluctuation of signal at the receiver due to the change of the refractivity of the propagating medium. The change of the refractivity may cause refraction of the beam or deviation of the beam away from its

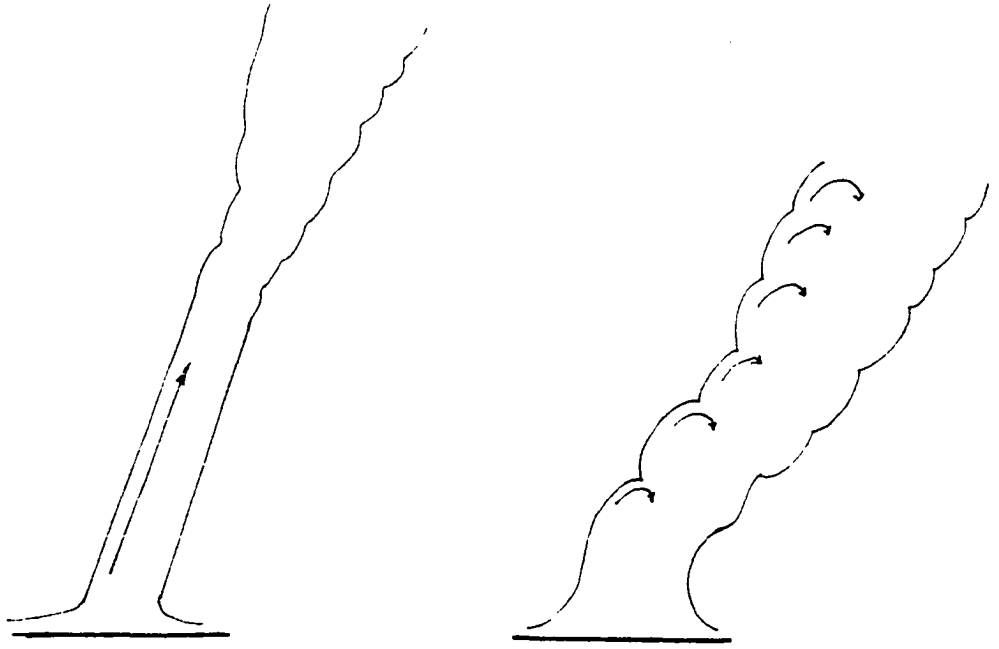

(a)
A plume blown by a small amplitude wind.

(b)
A plume blown by a strong wind shear.

Figure 3.2. Effects of horizontal wind on the thermal plane.

normal direction. The other expected effect is that a fluctuation of signal energy may result from the combination of the out-of-phase components of the wave at the receiver. The former case is likely to occur when the beam propagating through the plume is narrow in cross-section while the later case is more likely when the beam cross-section is broad.

IV. THEORY OF OPTICAL SCALING OF THE RADIO LINK

As mentioned in Chapter I, the frequency-scaling technique has been used by some researchers in studying certain electromagnetic wave phenomena. By using a laser as an electromagnetic source one can scale large-diameter antennas as small-sized antennas suitable for laboratory measurement. The theory behind this technique is that the dimensions of the antenna are scaled down by the ratio of the optical source wavelength to the wavelength of the actual source [19]. If we let S be the value of this ratio, which we will call the "scaling factor", then

$$S = \frac{\lambda_{Laser}}{\lambda_{Wave}} \tag{IV.1}$$

$$= \frac{L_{Laser}}{L_{Wave}} \tag{IV.2}$$

where λ_{Laser}, λ_{Wave}, L_{Laser} and L_{Wave} are wavelength and the path length of the laser model and the actual path respectively. In this experiment, a 6328 Å wavelength is used to simulate the transmitted wave and the scaling factor is about 6.328×10^{-6} if a 3 GHz wave is being simulated. The transmitter of the radio wave is simulated by passing the laser beam through a small aperture. The resulting beam will have the pattern of the Airy function, with the main lobe of approximately 1/8 inch in diameter at the receiver aperture.

The receiver of the model, which simulates the receiving antenna can be a photosensitive diode detector or a photomultiplier. The receiving area of the receiver simulates the aperture of the receiving antenna. With a very large value of scaling factor like this, the transmission path of a radio link can be shortened to a suitable length for the laboratory.

The refractivity ($N = (n-1) \times 10^6$, where n is the refractive index) of air at microwave frequencies is dependent upon its temperature, pressure and moisture content [20]:

$$N = \frac{77.6}{T} \left(p + 4810 \frac{e}{T}\right) \qquad \text{(IV.3)}$$

while the refractivity of air at optical frequencies is dependent upon its temperature and pressure only [21]:

$$N = \frac{77.6}{T} p \times 10^{-6}. \qquad \text{(IV.4)}$$

where p is the dry air pressure, e is the partial pressure of water vapour and T is the absolute temperature of the air.

The fluctuation of the received signal on a microwave radio link is due, mainly, to changes of moisture and temperature along the path whereas the fluctuation in the optical signal is caused by changes in the temperature alone. In either case pressure is not considered to be a significant contribution to short-term signal fluctuations. If the temperature of the air in the simulated path is controlled and changed in such a way that its movement is analogous to an atmospheric phenomena, then the fluctuation of the received signal will

be analogous to the signal characteristics of the radio link. By this means one can study the contribution of a particular atmospheric phenomena to the signal characteristics of a radio link.

As pointed out in Chapter III, the occurrence of the thermal plume in the natural environment is sufficiently common that one can expect it to occur in or to move past a radio link he is planning to establish. A question that should be answered is whether the role of thermal plume is such that its effects on the radio link should be considered in the design process. One way to do this more easily and economically than conducting an investigation on an actual propagation path is to model a thermal plume into a laboratory-size situation.

The scaling of the thermal plume to the model can be done in the following way. There are two parameters of the plume that affect the laser beam propagation; its size and its temperature gradients. Since the thermal plume has temperature higher than the surrounding air, there must be a temperature gradient outward in the radial direction due to conduction process as well as gradients caused by mixing.

The most desirable way to model the thermal plume would be to scale its size down while maintaining temperature gradients equivalent to those of the actual thermal plume. While it would be very difficult to make certain that the gradients due to mixing are modeled properly, it is not too difficult to ensure that the radially-directed gradients due to thermal conduction are scaled proportionately. As a very simple mathematical model, let us consider a column of heated air,

of circular cross-section; in thermal equilibrium with its surroundings. We can write the heat equation for this case as [22],

$$\nabla^2 T - \frac{c\gamma}{k} \frac{dT}{dt} = 0 \qquad \text{(IV.5)}$$

where T is the temperature, c is the specific heat constant, γ is the density and k is the thermal conductance of the air.

At steady state, that is when there is constant heat supplied to the cylinder of heated air, there will be no temperature changes with time in the plume, thus $\frac{dT}{dt}$ goes to zero, and

$$\nabla^2 T = 0. \qquad \text{(IV.6)}$$

Assuming that there is no temperature change in the vertical nor circumferential directions; $\frac{\partial T}{\partial z}$ and $\frac{\partial T}{\partial \phi}$ are zero, and the heat equation becomes (in a cylindrical coordinate system)

$$\frac{1}{r} \frac{\partial}{\partial r}\left(r \frac{\partial T}{\partial r}\right) = 0. \qquad \text{(IV.7)}$$

From the above equation we have

$$r \frac{\partial T}{\partial r} = c_1 \qquad \text{(IV.8)}$$

where c_1 is a constant, or

$$\frac{\partial T}{\partial r} = \frac{c_1}{r}. \tag{IV.9}$$

A solution to the equation (IV.9) is

$$T = c_1 \ln r + c_2 \tag{IV.10}$$

where c_2 is another constant.

Let T_0 be the temperature of the surrounding air at a distance R away from the thermal plume. Thus,

$$T_0 = c_1 \ln R + c_2 \tag{IV.11}$$

The temperature at the periphery of the thermal plume is T_1, so we can write

$$T_1 = c_1 \ln a + c_2 \tag{IV.12}$$

where "a" is the radius of the thermal plume. The difference in temperature of the thermal plume and the surrounding air is then,

$$\Delta T = c_1(\ln a - \ln R) \tag{IV.13}$$

or

$$\Delta T = c_1 \ln a/R. \tag{IV.14}$$

From equation (IV.14) we have

$$c_1 = \frac{\Delta T}{\ln a/R}$$

$$= - \frac{\Delta T}{\ln R/a} \qquad \text{(IV.15)}$$

Substitute c_1 into equation (IV.8),

$$T = - \frac{\Delta T \ln r}{\ln R/a} + c_2 \qquad \text{(IV.16)}$$

and from equation (IV.11), substitution of c_2 gives,

$$T = T_0 + \frac{\Delta T}{\ln R/a} (\ln R - \ln r) \qquad \text{(IV.17)}$$

or

$$T = T_0 + \frac{\Delta T \ln R/r}{\ln R/a} \qquad \text{(IV.18)}$$

Substituting c_1 into equation (IV.9) gives,

$$\frac{\partial T}{\partial r} = - \frac{1}{r} \frac{\Delta T}{\ln R/a} \qquad \text{(IV.19)}$$

By the same procedure, the temperature gradient for the model plume can be written as

$$\frac{\partial T'}{\partial r} = - \frac{1}{r} \frac{\Delta T'}{\ln R/a} \qquad \text{(IV.20)}$$

where T', a', and r' are the temperature, the radius and the radial distance from the center of the model plume respectively.

In order to make the temperature gradient at the periphery of the thermal plume and the model plume be equivalent to each other and to introduce the scaling factor, S, as we scale down the wavelength of the wave, we have

$$\left.\frac{\partial T'}{\partial r}\right|_{r = a'} = \frac{1}{S} \left.\frac{\partial T}{\partial r}\right|_{r = a} \tag{IV.21}$$

or

$$-\frac{1}{a'} \frac{\Delta T'}{\ln R/a'} = -\frac{1}{S} \frac{\Delta T}{\ln R/a} \cdot \frac{1}{a} \tag{IV.22}$$

Solving for $\Delta T'$ results in

$$\Delta T' = \frac{a' \ln R/a'}{Sa \ln R/a} \cdot \Delta T \tag{IV.23}$$

Now take the limit as R becomes infinitely large

$$\lim_{R \to \infty} \Delta T' = \lim_{R \to \infty} a' \frac{\ln R/a'}{Sa \ln R/a} \cdot \Delta T$$

$$= \frac{1}{S} \cdot \frac{a'}{a} \cdot \Delta T \tag{IV.24}$$

Equation (IV.24) shows the relationship between the temperature differences of the modeled plume and the natural plume. In the model,

a' is 1.27 cm, $\Delta T'$ is about 110° C, ΔT is about 2° C, and, assuming that S is 10^{-6}, a is about 204.54 m. This means that our model is a simulation of a large sized thermal plume.

V. EXPERIMENTAL SET UP AND PROCEDURE

V.1. The Set Up

The model used in this experiment consisted of four principal parts: the supporting structure, the laser head and the receiver, the optical apparatus and the equipment designed to produce the simulated atmospheric turbulence.

The experimental set up was situated on a wooden surface supported by steel legs imbedded in solid concrete blocks. The entire structure was enclosed in styrofoam paneling to prevent the outside air from interfering with the atmosphere within the path of the laser beam. The concrete blocks were intended to stabilize the whole structure. Figure 5.1 is the photograph of the experimental set up.

The laser, used in this experiment as a source of electromagnetic waves, is a Spectra Physics Model 120 helium-neon gas laser. This laser is capable of producing an output of 5 mW at a wavelength of 6328 Å; which is visible as a red-colored beam. The laser is operated in the TEM_{00} mode in order to produce a uniform-phase wavefront.

The receiver used to detect the energy of the laser beam consists of a solid-state photodiode detector and a preamplifier. The photodiode is the SDG-100A. The signal detected by the diode is then amplified by a dc preamplifier. A schematic diagram of the receiver circuit is shown in figure 5.2. The signal then passes to the preamplifier of a Sanborn chart recorder which recorded the signal fluctuations on a paper record.

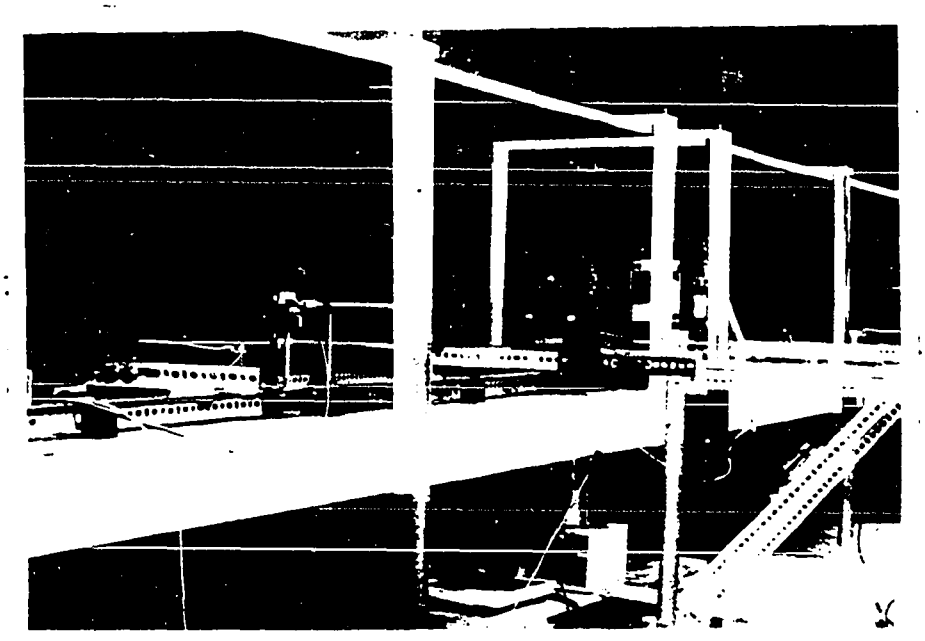

Figure 5.1. The photograph of the experimental set up.

The optical apparatus consists of two concave mirrors, a spatial filter, a beam divider, two planar mirrors, a polarizing filter and a small aperture. The arrangement of the optical apparatus is shown in figure 5.3.

The atmospheric turbulence generator is constructed as shown in figure 5.4. It consists of a hot air storage tank, a gating shutter and a blower. A heating element is located inside the hot air storage tank to heat the air in the tank. The blower is connected to the tank through a section of tubing to a hole in the bottom. The blower increases the pressure in the tank; hence speeding the air flow upward. An aperture which can be opened and closed by means of a solenoid-actuated shutter is located at the top of the tank. This

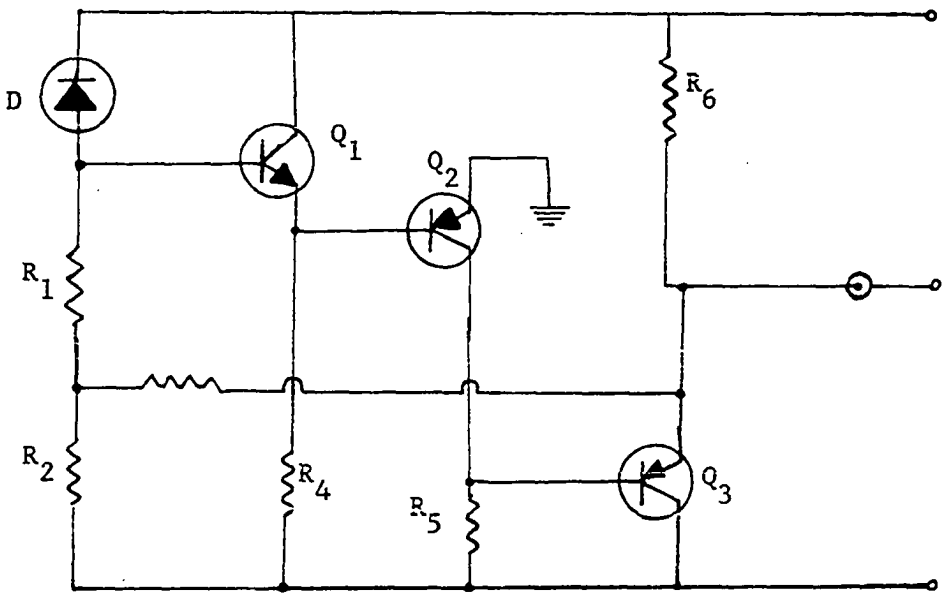

D = Photodiode, SDG-100A

Q_1 = Transistor, 2N2484

Q_2 = Transistor, 2N3251

Q_3 = Transistor, 2N3251

R_1 = 10 M

R_2 = 10 M

R_3 = 200K Pot.

R_4 = 10 M

R_5 = 470K

R_6 = 100K

Figure 5.2. The schematic diagram for the receiver.

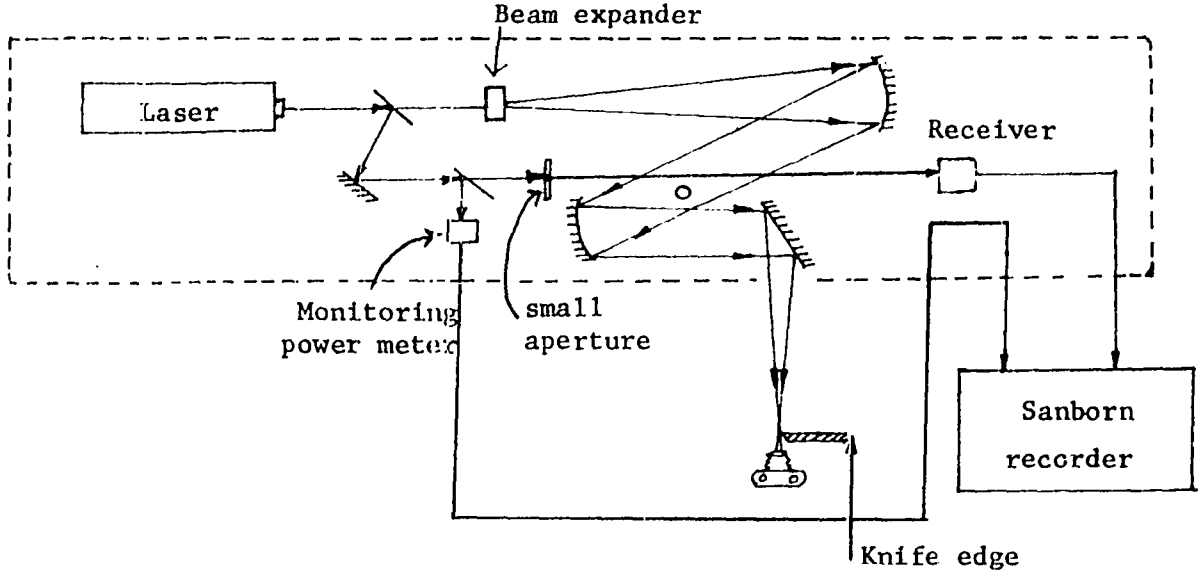

Figure 5.3. The arrangement of the experimental set up.

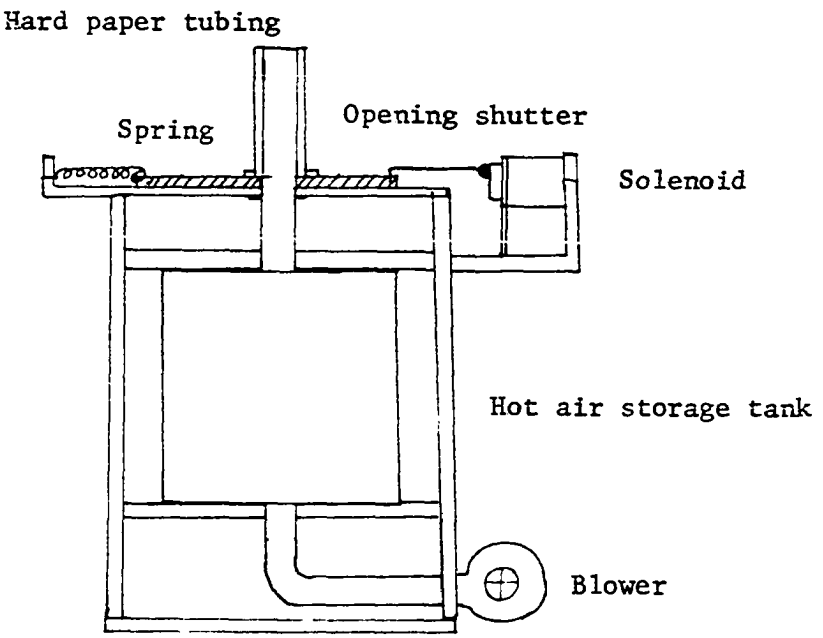

Figure 5.4. The thermal plume generator.

machine is intended to be used to generate hot air bubbles or a thermal plume. In order to get a good smooth upward flow of heated air, a one-half inch diameter hard paper tube is attached to the aperture on the shutter assembly. A piece of masonite with a hole for the tube covers the entire structure to prevent other air currents from interfering with the thermal column.

V.2. The Calibration and Testing of the Instruments

Before the experimental procedure can be performed, the equipment described in section VI.1 must be checked and calibrated. For example, the laser must be monitored to see that during the course of the experiment the fluctuation of the signal is not caused by fluctuations of the power output of the laser itself. The receiver must be checked for linearity of detection and calibrated for the received signal levels. Finally, the thermal plume generator must be checked to make sure that it really produces a plume which is a good simulation of the atmospheric thermal plume.

The power level of the laser was monitored by using a Spectra Physics model 401B power meter to measure the output of the laser at one of the divided beams. The signal was fed to the preamplifier of the second channel of the Sanborn recorder so that the signals from both the direct and the monitoring channels were recorded simultaneously. Figure 5.3 shows the diagram of power monitoring arrangement.

The linearity of the receiver was checked by passing the laser beam through a polarization rotator capable of rotating the polarization of the beam through 360 degrees. A beam chopper was placed in the light path after the polarization rotator to chop the laser beam at the rate of 900 times per second. At the receiver, a polarizing filter was inserted in front of the aperture so that the receiver would measure only the component of the polarization matching that of the filter. The output of the receiver then was connected to an ac microvoltmeter. The block diagram of the arrangement for the testing is shown in figure 5.5.

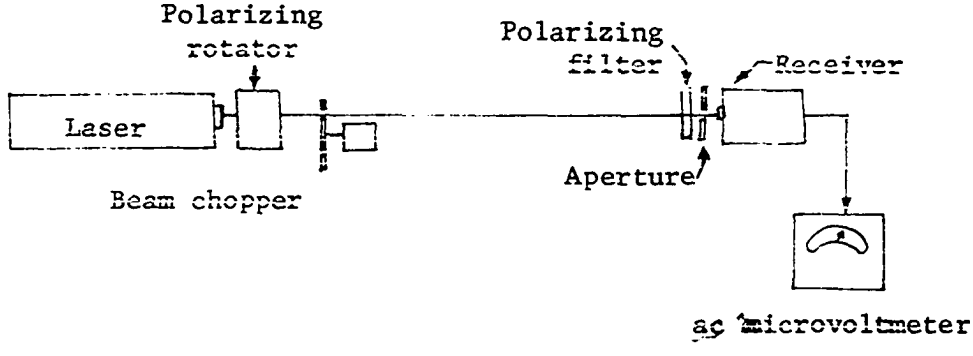

Figure 5.5. The block diagram of the receiver linearity testing system.

During the test, the polarization of the laser beam was rotated through 5 degree increments and the reading of the ac microvoltmeter was recorded, the total range of 720 degrees of rotation was covered in this process. The data was plotted with the meter reading versus the polarizing angle. A theoretical curve of the received power versus the polarizing angle was plotted on the same graph for comparison. The theoretical curve is that generated by the equation: $E_{max} \cdot \sin^2\phi$ for the range of the angles of polarization, where E_{max} is the maximum value of the meter reading and ϕ is the angle of polarization. The two curves are plotted as figure 5.6, from which we can see that the experimental curve closely resembles the theoretical curve, except for small deviations at the upper and lower portions of the curve. It is seen that the receiver operates in linear proportion to the incident power in the range between 10 mV to 72 mV. This characteristic curve limits the use of laser beam power to this linear region. This can be done by using a neutral filter to reduce the beam intensity.

The Sanborn recorder was checked for linearity of its chart record by feeding a triangular wave from the Beckman function generator model 9030 into its preamplifier. The output voltage of the triangular wave generator was adjusted so that the swing of the recorder stylus stayed within the limits of the recording chart. The two channels of the recorder were checked simultaneously. A portion of the chart record is shown in figure 5.7. From the figure we can see that the record is linearly related to the input voltage over almost the entire width of

Figure 5.6. The plot of the voltage reading versus the angle of polarization compared to the theoretical plot, for the linearity testing of the receiver.

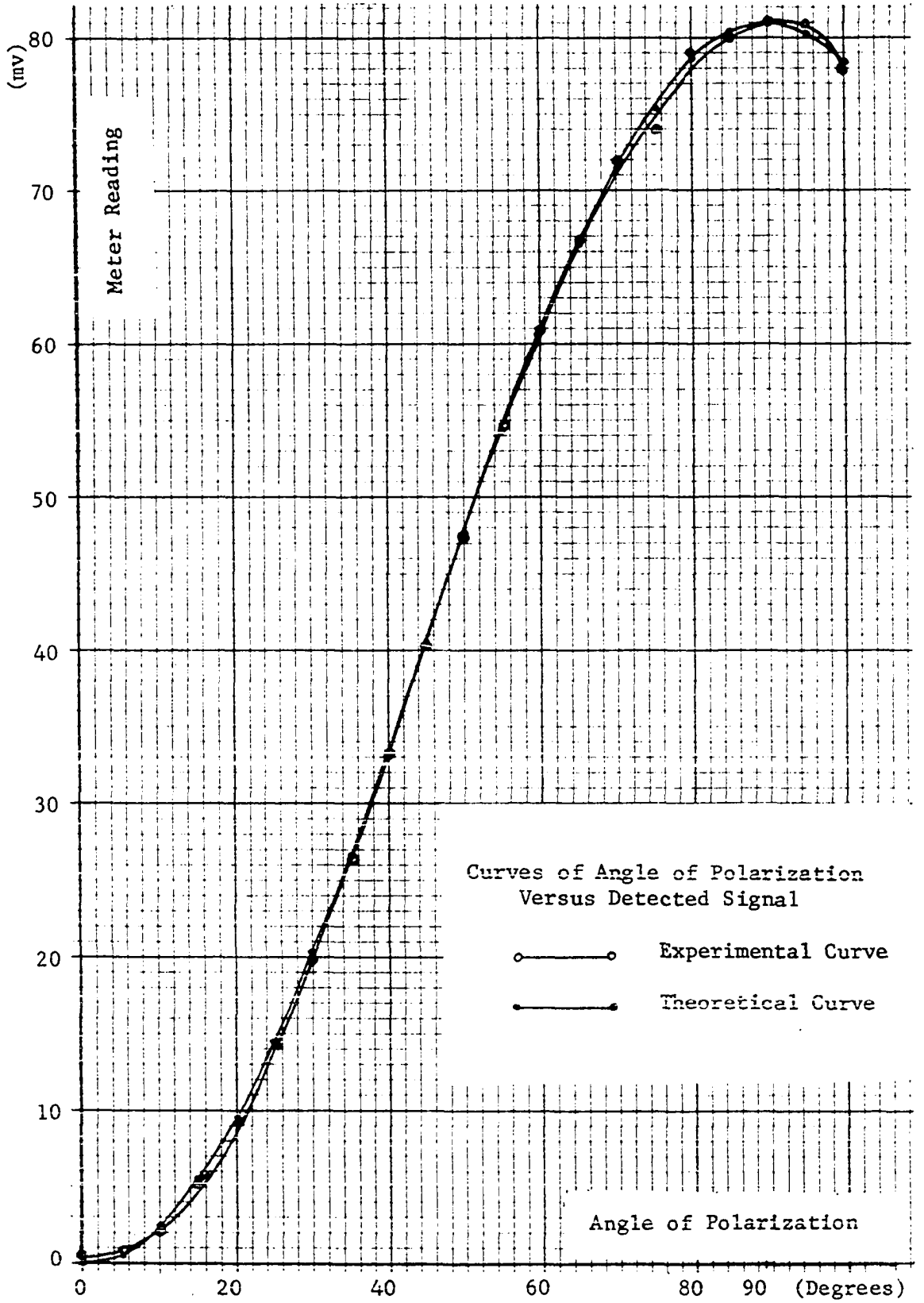
(mv)
80
70
60
50
40
30
20
10
0
Meter Reading
Curves of Angle of Polarization
Versus Detected Signal
Experimental Curve
Theoretical Curve
Angle of Polarization
0
20
40
60
80
90
(Degrees)

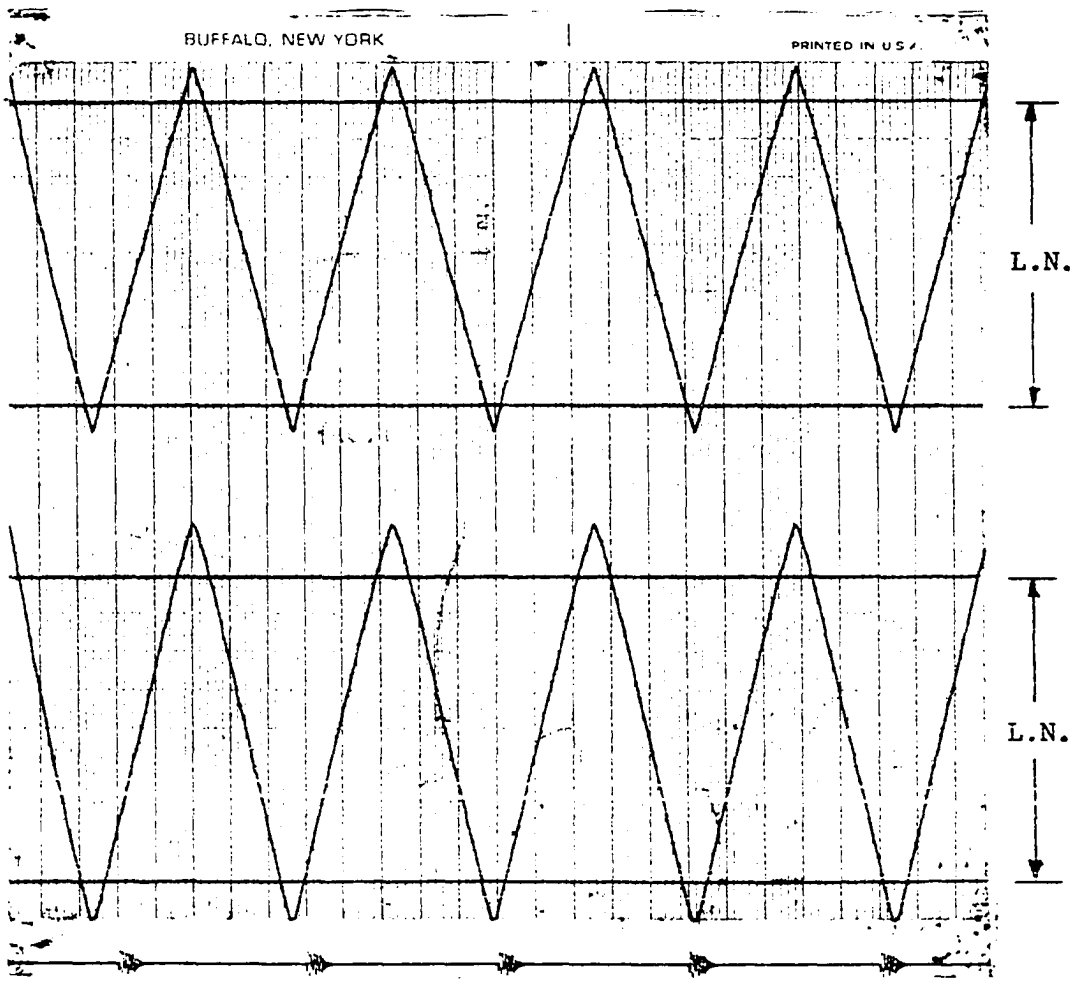

Figure 5.7. The recorded signal for the linearity testing of the Sanborn recorder.

the chart for both channels. Thus we can assume linearity of the recorder to a very good approximation. For added assurance, only the portion "L.N." of the chart shown in figure 5.7 was used in the experiments.

The calibration of the chart record for the signal degradation in decibels was done by using a calculation from the equation

$$10 \log_{10} \frac{E_m}{E_i} = F^{dB} \qquad (V.1)$$

where E_i is the instantaneous voltage and E_m is the maximum voltage when there is no disturbance, and F is the depth of the fade in decibels. Since the receiver and the recorder are operating in a linear region, the divisions on the recorder are proportional to the detected voltage which is, in turn, proportional to the incident power on the diode. The maximum swing of the recording needle is adjusted at 3 large divisions on the chart record. From equation (V.1) the calculation of the divisions of the chart record corresponding to the number of decibels of signal fade detected is determined by

$$D_i = \text{anti } \log_{10} \left(\frac{F^{dB}}{10}\right) \cdot D_m \qquad (V.2)$$

where D_i and D_m are the instantaneous and maximum deviation of the needle from no signal level. And F^{dB} is the number of decibels of

signal fade. The deviation of the needle below the maximum is then equal to $D_m - D_i$. Table V.1 shows the fades on a chart record corresponding to the number of decibels.

Table V.1. An example of chart calibration data.

F^{dB}	Division on chart below the maximum level
1	0.617
2	1.108
3	1.497
4	1.806
5	2.052
6	2.247
7	2.402
8	2.525
9	2.622
10	2.703

An example of the chart calibration is shown in figure 5.8.

To ensure that the plume emerging from the generator be a close approximation to the natural plume, smoke was introduced into the tank so that its trace could be observed and photographed. Several schlieren pictures were taken for study.

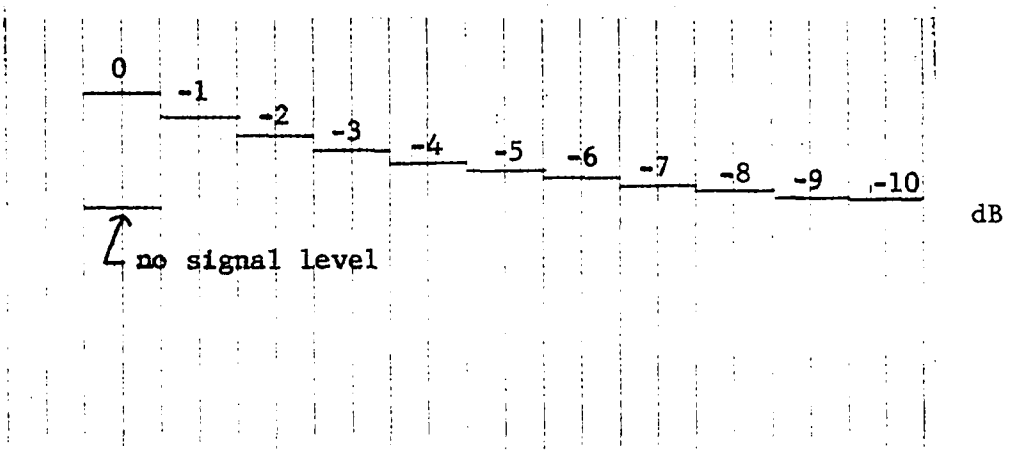

Figure 5.8. The calibrated chart, in decibels.

Figure 5.9 is a photograph of the smoke tracing of a simulated thermal plume. The warm air rises in the form of a column before it

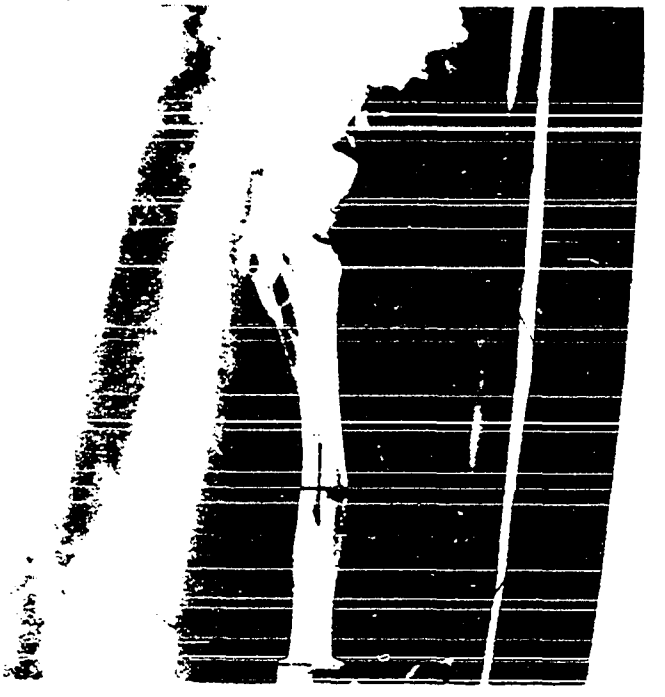

Figure 5.9. Trace of the generated plume showing a close resemblance to an atmospheric plume.

begins to break up into turbulence. From the picture we can see that the flow is almost laminar; that is, the streamlines are almost parallel to each other. The twisting of some streamlines may be due to small disturbances of the air surrounding the plume. Figure 5.10 shows the perturbed flow when a horizontal wind blows from the left. We can see the eddies of the flow quite clearly. From the picture we can state that the plume does not break up and lose its identity; but, still flows although with more turbulence evident. Figure 5.11 shows the plume with a small tilt when the wind blows with less strength than in figure 5.10. We can see that the plume, after bending a little, continues to flow upward with some eddies forming to the right side of the plume. The upper portion of the plume has become fully occupied by eddies. From these photographs, we can see that the generated plume closely approximates the atmospheric thermal plume; it rises up in the form of a column and its flow is quite uniform.

V.3. The Experimental Procedure

After all the instruments were tested and calibrated so that their operational characteristics met the necessary requirements, the experiment was performed by arranging the instruments as shown in figure 5.3. As shown in the figure, the laser beam was divided into two beams by a beam splitter, one beam was expanded by a spatial filter and used as a light source for the schlieren system. The other beam was divided again by another beam splitter into two beams, one passed through a

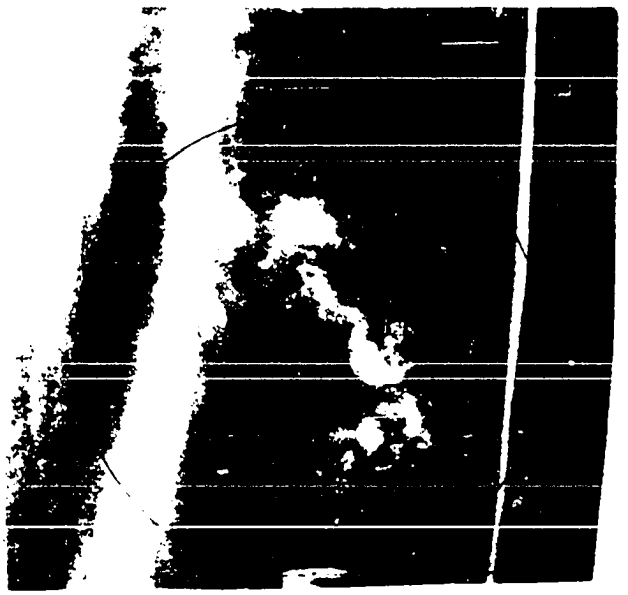

Figure 5.10. Trace of generated plume, showing the effect of a horizontal wind from the left.

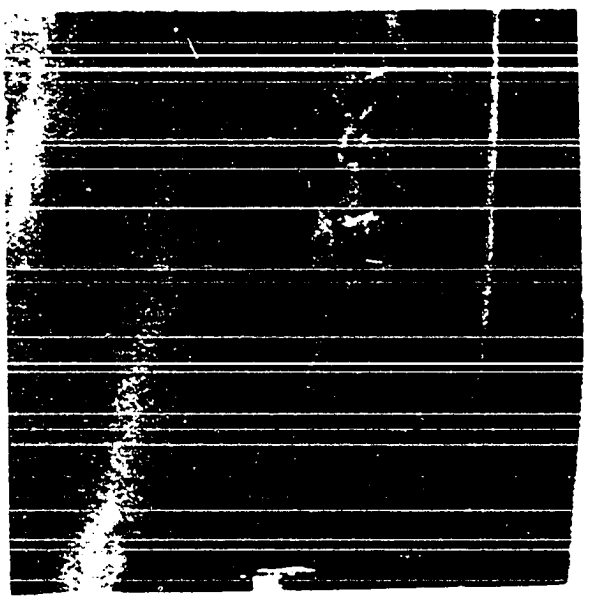

Figure 5.11. Trace of the generated plume, showing the tilting effect by horizontal wind at low speed.

small aperture to the receiver while the other one passed to the detector of the power meter used to monitor the output power of the laser.

The thermal plume generator, as shown in figure 5.4, was located in the middle of the path between the small aperture and the receiver. It was leveled so that its outlet, one end of the hard paper tube, was just above the level of the hardboard cover and projected into the schlieren field only about 0.5 cm. Figure 5.12 is a side-view diagram of the arrangement to show the level of the different instruments.

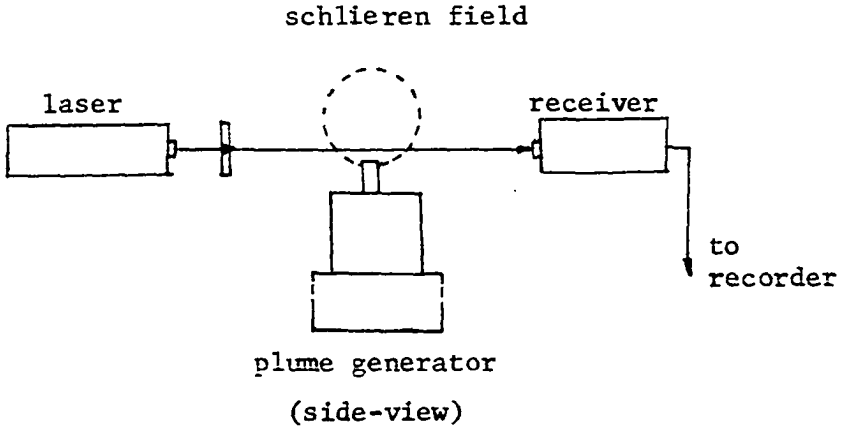

Figure 5.12. The location of the thermal plume generator.

During the experiment, the outlet for the warm air was left open all the time to produce a column or plume of heated air. The blower was not turned on, since it tended to produce turbulent air flow instead of the uniform flow required. The heater was turned on and allowed to heat the air in the tank. The temperature of the air in the tank was monitored by a Simpson model 388 thermocouple thermometer.

The warm air was then allowed to flow freely out of the chimney and into the schlieren field.

The adjustment of the schlieren system was a very important and difficult process. The beam passing through the spatial filter must be adjusted so that it is free from interference patterns and expanded to the proper size. The spatial filter, which is composed of a microscope objective lense and a pinhole, must be selected so that it produces an expansion of the beam to the size of the concave mirror. This is to prevent the loss of beam energy resulting from too much expansion, yet allowing the largest schlieren field possible. We chose a 10X microscope objective and a 25μ diameter pinhole as components of the spatial filter. This combination delivered a very clean beam expanded to the proper size to the first concave mirror of the schlieren system; which was placed at the distance equal to its focal length from the spatial filter (60 inches). The first concave mirror then was adjusted to reflect the beam, which was collimated at this point, to the second mirror. The beam must pass through the test section as shown in figure 5.3. The beam then was reflected out of the box by a plane mirror to a screen or a camera. At the focus of the second mirror a knife edge was used to block a part of light beam to increase the sensitivity of the system to changes in the density of the air in the test field. The knife edge used in this experiment was a razor blade edge. By means of a precision translator, the knife edge could be moved in the horizontal direction perpendicular to the axis of the beam which

was reflected from the second concave mirror. The knife edge was moved into the path of the beam to block a portion of it, as shown in figure 5.3. In this experiment several positions of the knife edge were tried, and it was found that the most suitable position covered about 1/10 of the diameter of the beam.

Taking the schlieren photographs of the test field was different from the other instances reported in the literature [23, 24, 25], since most of these recommended a large film format type of camera. This type of camera would be very convenient to use with this experiment, since its plate holder could be moved to a proper distance from the lens so that a suitable size of picture could be taken. In our experiment we need a camera with a shutter speed of not less than 1/500 second. This limitation was found experimentally by taking a series of schlieren photographs at different shutter speeds. The best picture, in terms of exposure and stopping action, was the picture that was taken with a shutter speed of (1/500)s. Since a large format camera with high speed shutter is very hard to find on this campus, we decided to use an available single lens reflex Asahi Pentax model SV camera for photographing the schlieren field. The camera was set on a tripod and an air-pressure-operated cable release was used to trigger the camera shutter. The first set of the pictures were taken with a 55 mm focal length lens on the camera, placing the lens just behind the knife edge as was done by other authors [23, 24, 25]. The resulting pictures were too small. Another set of pictures taken with the lens removed; that is, by letting the

light beam fall directly upon the plane of the photographic plate. The size of the picture could be adjusted by moving the camera away from the focal point of the concave mirror to a proper distance as determined by looking through the view-finder of the camera. After the camera was properly positioned, the film was loaded, the shutter speed set, and the shutter cocked so that it was ready to take a picture at the precise moment of signal fade.

At the Sanborn recorder, the output of the receiver was connected to the input of the first channel of the preamplifier, the attenuator and the sensitivity were adjusted so that the total swing of the stylus, from beam on to beam off, was three large divisions of the chart record. While the beam was on, the centering controls were adjusted so that the needle rested on the line of the second large division of the chart record from the top of the chart. This was selected to be the 0 dB level on the chart. The second channel of the preamplifier was fed with the signal from the power meter which monitored the power of the laser beam. The attenuator and sensitivity were adjusted so that the noise from unknown sources in the building which was picked up by the line was suppressed. The stylus then was adjusted to rest on the line of the third large division of the chart record, while the beam was on.

When the experiment was performed, the recorder and the plume generator were operating, the signal level of the first channel was visually monitored, and the shutter release was readied to be actuated. When the stylus of the recorder indicated a low signal level, the shutter was released at once and then reset for another picture. The

experiment continued until the camera ran out of film (about 20 exposures). Approximately 15 rolls of film were exposed during the experiment. Some of the better pictures are shown in this report.

At the outset of the experiment it became apparent that the plume did not produce significant low level fades, but later experiments determined that the introduction of a horizontal wind to move the plume across the testing beam produced considerable low level fading of the signal. The equipment used to produce the horizontal wind consisted of a small blower placed about 6 feet from the thermal plume with a wooden shutter to block or release the wind into the test area at convenient times.

After a series of narrow beam experiments were performed the test beam was expanded by replacing the small aperture with a lens. The same procedure of experimentation was run, but no low level fading was evident.

VI. RESULTS

The results of the experiment are shown as signal records and schlieren pictures in figures 6.1 through 6.8. The signal records are those which show low level fades, and the pictures are the corresponding schlieren pictures at the moment of fading. There are several records in which the amplitude fluctuations are small. These are not shown here. Figure 6.1 shows the plume rising with a very little disturbance. It exhibits a little tilt and its boundary cuts through the path of the test beam. The density gradient of the air parcel in the plume and the outside air produced a refraction of the beam; thus causing the signal level at the receiver to fluctuate. The recorded signal on the Sanborn chart recorder is shown below the schlieren picture in the same figure. The fading of the signal is about 2.0 dB at the moment of taking the picture at the arrow, while another fade of about 5 dB is recorded just a few seconds behind it. The time scale is shown in the lower part of the chart with each division equal to a one second interval.

Figure 6.2 shows the thermal plume model being blown by the horizontal wind from the right. This time the wind was strong enough to cause the column of the plume to break up into many eddies. Since the eddies consist of warm air from the plume mixing with the outside air, the density gradient of the plume is quite sharp and caused the fading of the signal as shown in the signal record below the picture. Figure 6.3 is another schlieren picture taken at the

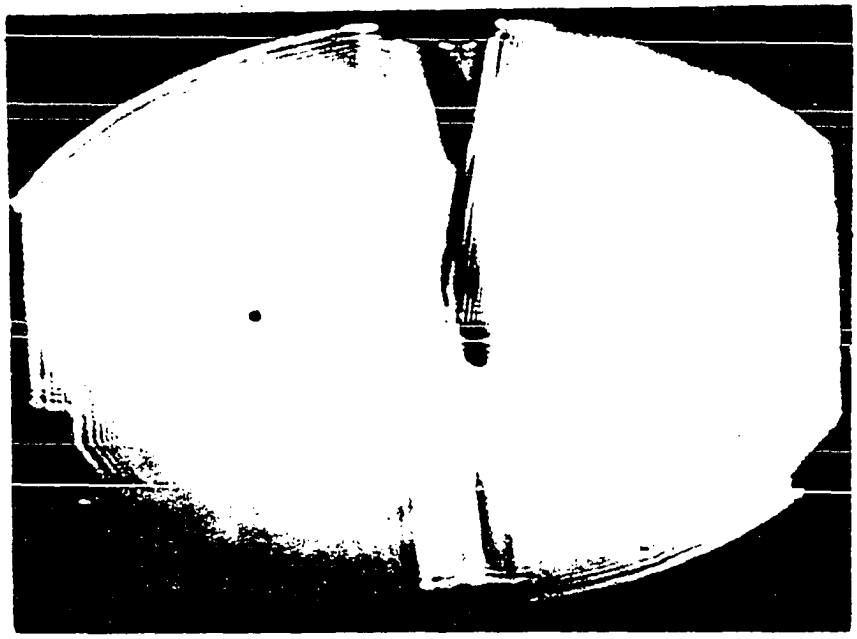

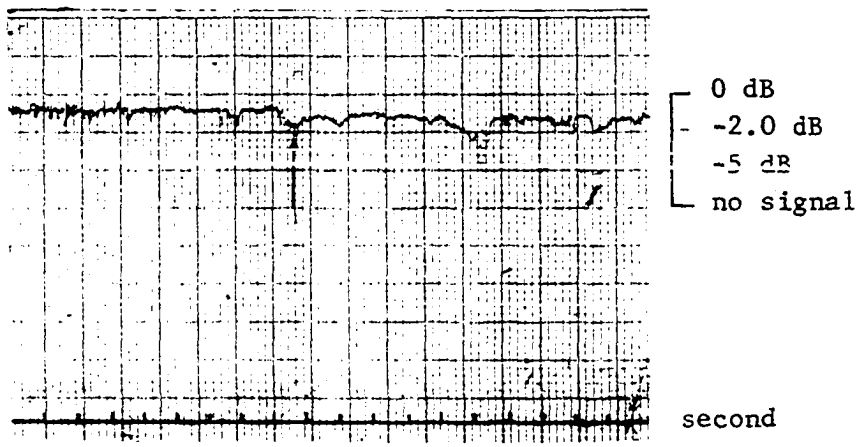

Figure 6.1. A schlieren photograph of the modeled plume and a recorded signal, showing the effect of the plume in vertical position in the path of a radio link.

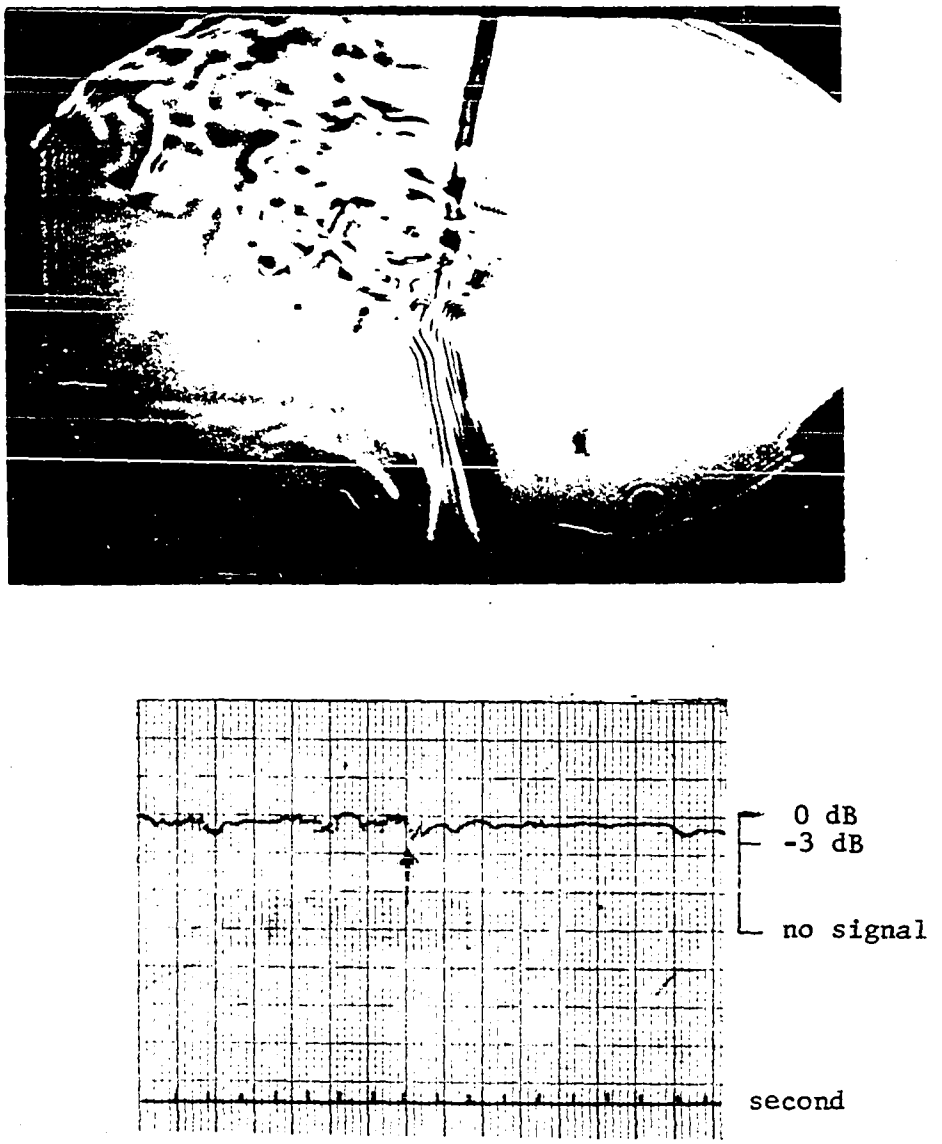

Figure 6.2. A schlieren photograph of a thermal plume and the recorded signal, showing the plume being blown from the right.

moment of fading, with its signal record shown below it. This figure is the same as figure 6.2; that is, the plume was affected by a horizontal wind shear. Figure 6.4 shows the plume being blown by a low velocity wind. The horizontal velocity vector did not create any vorticity at the boundary of the plume; it just caused the plume to tilt. It is evident that only the top portion became turbulent. The signal record is shown below the schlieren photograph. Notice that the zero level of fading is at the third large division of the chart record.

Figure 6.5 is another schlieren photograph of the model plume tilting a little to the left and causing a fading of the signal as shown on the chart record below the schlieren photograph. The fade level at the arrow indicating the moment when the photograph was taken is about 2 dB. In this instance, the effect of the plume is to produce a set of repetitive fast fades combining into a slower fade. Figure 6.6 shows a plume being broken up at the top portion by the fluctuation of a horizontal wind. The portion of the plume in the neighborhood of the path of the test beam contains some eddies, and the passage of these eddies across the beam cause the fast fading of the signal as shown in the chart record below the photograph. The fade level at the point of taking this photograph is about 1 dB which is small. Figure 6.7 shows a modeled plume with its top portion being broken into eddies, but with fewer eddies than in the case of figure 6.6. Its fading characteristic, shown below the photograph, is different from that of figure 6.6. In this

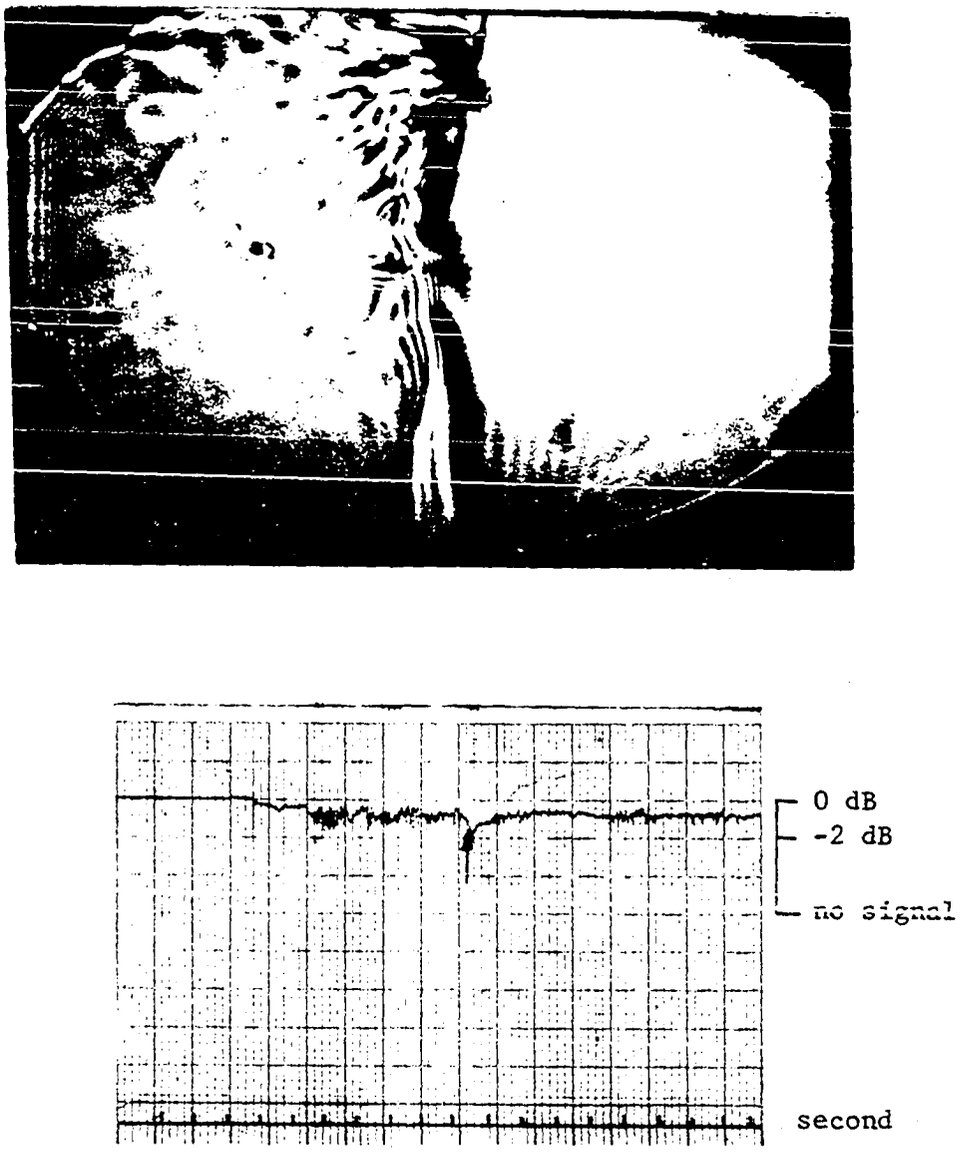

Figure 6.3. A schlieren photograph of a modeled plume signal and its fading signal below.

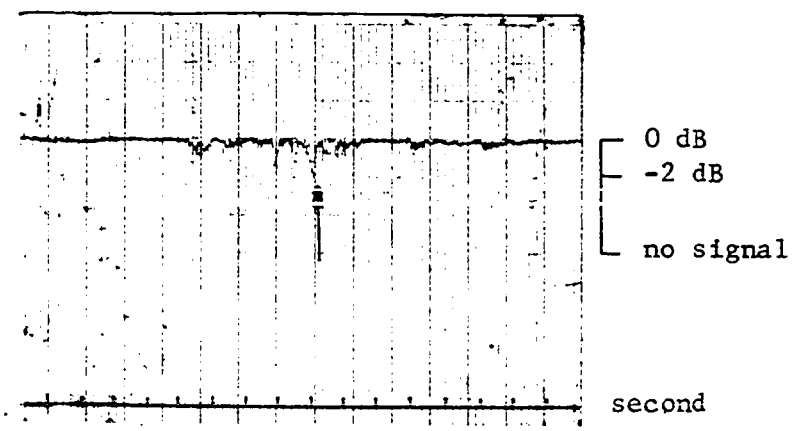

Figure 6.4. A schlieren photograph of a plume being blown by a horizontal wind at low speed and its recorded signal.

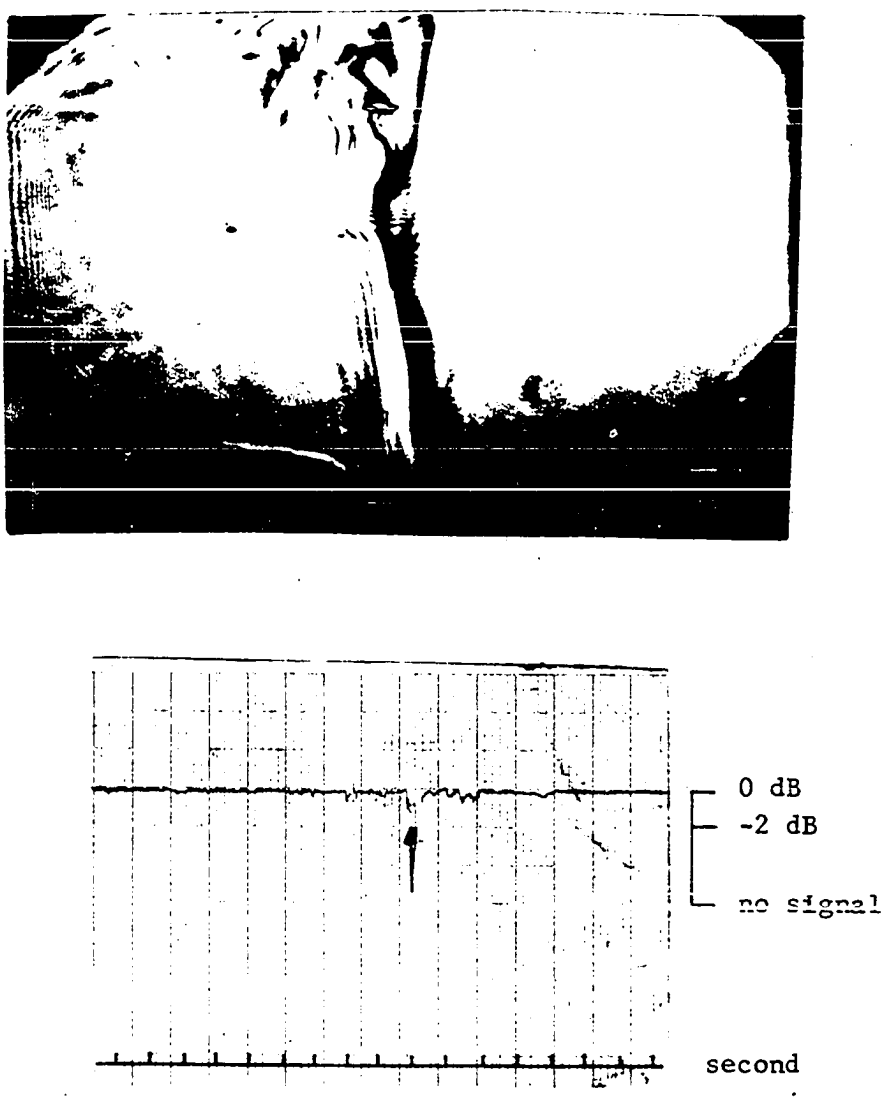

Figure 6.5. A schlieren photograph of a thermal plume tilted from the right passing the test beam, and its recorded signal.

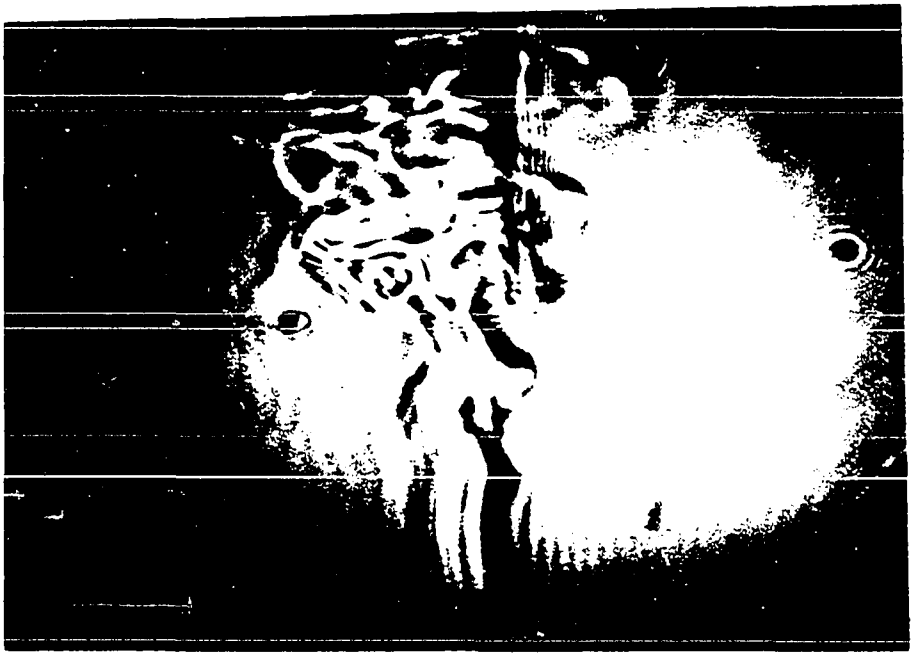

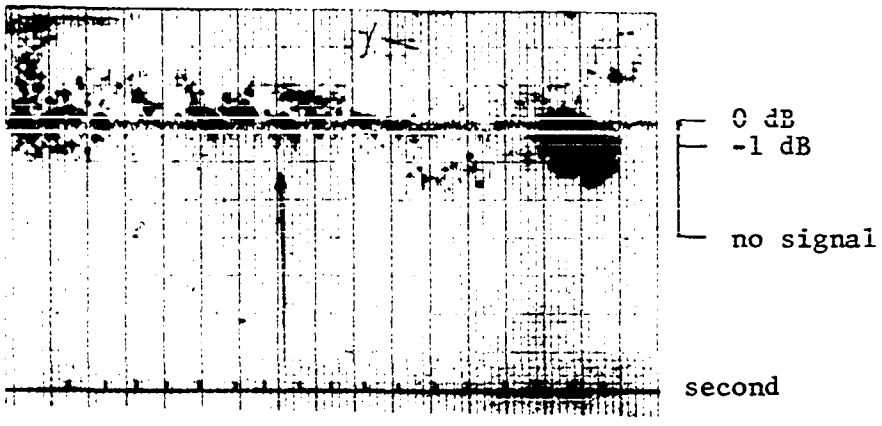

Figure 6.6. A schlieren photograph of a plume being broken up at the top portion and fading characteristic below.

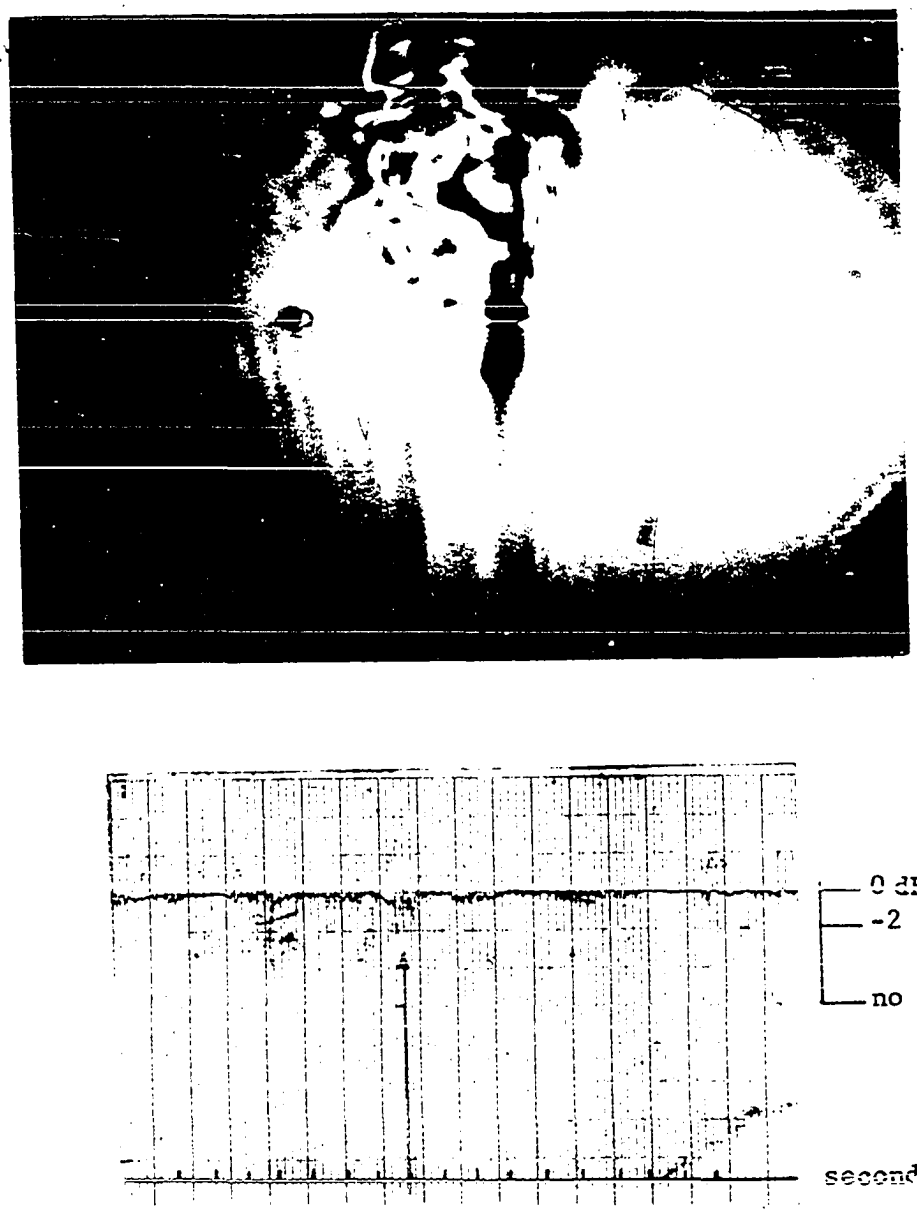

Figure 6.7. A schlieren photograph of a modeled plume with top portion in turbulence and its fading characteristic.

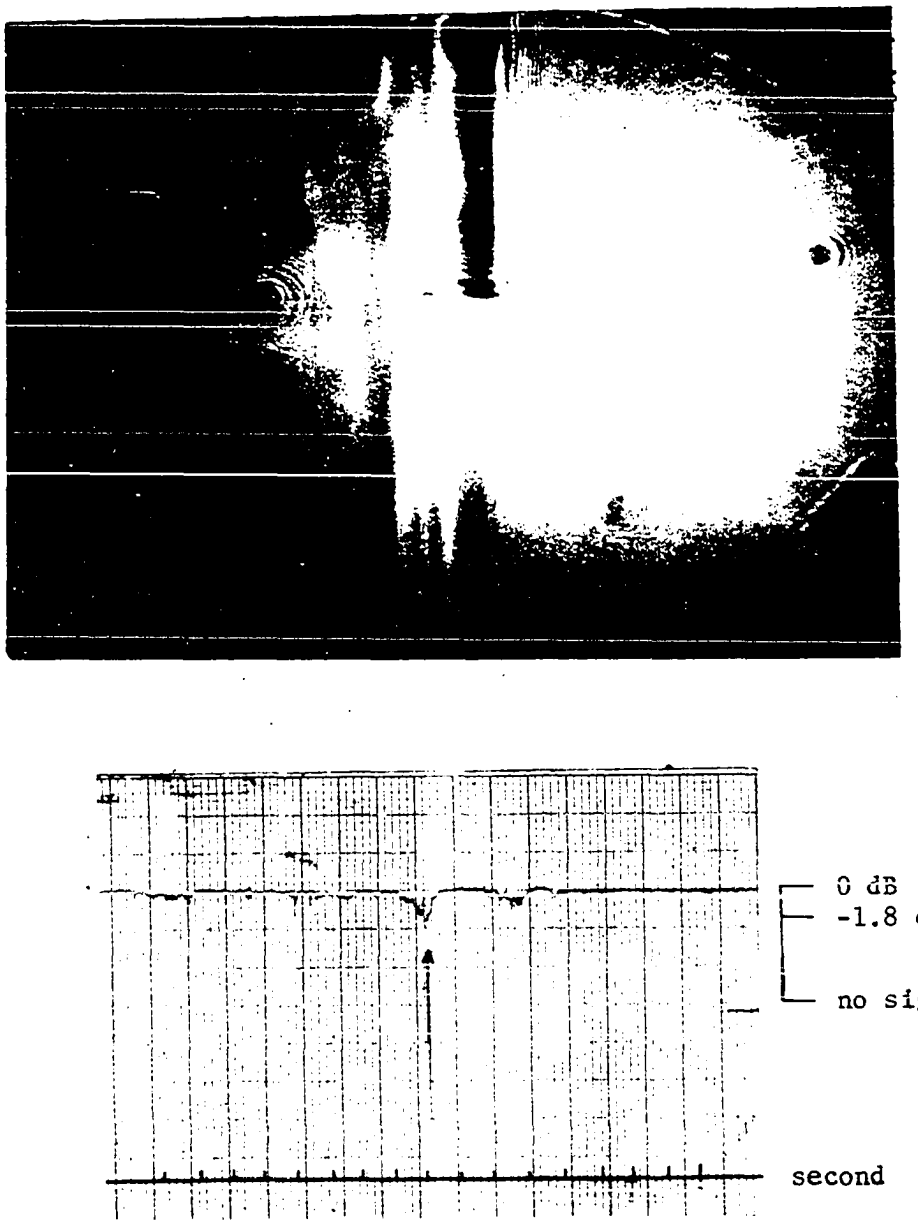

Figure 6.8. A schlieren photograph of a modeled plume with a straight up position and its fading characteristic.

figure, the fade level at the time of the taking of the photograph consists of several fast fades combined into a set of slower fades as in figure 6.5. The fade level is about 2 dB at that point. Figure 6.8 is another schlieren photograph of the model plume in a straight-up position. Its fading characteristic is similar to that of figures 6.1, 6.2 and 6.3; it is a slow fade with very small number of fast fades superimposed. The level of fade in this case is about 1.8 dB.

VII. CONCLUSION

The results of this experimental investigation demonstrated the feasibility of the scaling technique for the simulation of the effects of a thermal plume on a line-of-sight radio link. It also shows the possibility of applying techniques similar to those used in this investigation to study other atmospheric phenomena which, at least theoretically, are supposed to have some effect over the line-of-sight radio wave propagation process.

From the experiment, the deepest level of signal fade is about 5 dB, this rarely occurred. The signal fade level of about 1 to 2 dB occurred in the majority of the cases. The fading of the signal strength due to the effect of a thermal plume was never such that it could be classified as a deep fading (> 10 dB) mechanism. However, a deep fade may occur on a radio link by the multiple effects due to more than one thermal plume.

It should be noted that three distinct fading characteristics were obtained from this experiment. One type of fading is the fast fading as indicated at the beginning of signal records in figures 6.1, 6.3 and 6.6. This type of fading may be caused by the moving of a number of small sized inhomogeneities of the air parcel across the beam with relatively high speed. The level of signal fade is quite low for this type of fading (approximately 2 dB).

A second type of fading is the one which begins with a slow descending of the signal level to a fade level of about 1 to 2 dB and then

suddenly exhibits a fast fading characteristic at the lower signal level. Examples of this effect are seen in the later portion of the signal records of figures 6.1, 6.4, 6.5 and 6.7. This type of fading may be caused by a process wherein the boundary of the plume moves slowly through the beam followed by a number of thermally inhomogeneous air parcels or possibly an irregular surface plume moves past. After that the boundary moves back into the beam again. This type of fading produces a deeper fade level than the first one. From the experiment, the lowest fade level is about 5 dB in figure 6.1 and about 1 to 2 dB in the majority of cases where this type of fading was evident.

The third type of fading is the slow fade which begins with a lowering of signal slowly to the fade level of about 1 to 2 dB and then returning to its normal level. The fading characteristic is almost like an inverted triangle, as shown in figures 6.1, 6.2, 6.3 and 6.8. This type of fading may be caused by the moving of a smooth boundary of a plume into the beam and refracting the beam away from the receiver. It is possible that this type of fading combines with the first type at the tip of the inverted triangle to result in the second type of fading; which in some cases can be a severe one.

The experiment using the broad beam cross section did not result in any evidence of severe fading. The small amplitude fluctuations which were observed are theoretically caused by the combination of the out of phase components of the signal at the receiver. As in the case of narrow beam propagation, the multiple occurrence of the thermal

plume is possible, thus a lower level of signal can be expected at the receiver in the real world.

From the results of the two types of beam propagation experiments, another conclusion can be drawn. This is, the main effect of the thermal plume is to refract or deflect the narrow beam away from the line-of-sight path. This conclusion supports the report made by Waterman, when he performed a swinging beam propagation experiment. He stated that there must be some kind of scattering volume, refracting layer or a wave-like moving medium between the transmitter and the receiver [26]. The thermal plume or plumes may be the cause of the refracting medium he mentioned.

VIII. BIBLIOGRAPHY

1. Skolnik, M.I., "A Method of Modeling Array Antennas," IEEE Trans., vol. AP-11, 1963, pp. 97-98.

2. Redlien, Henry W., Jr. and Heinemann, Herman M., "Optical Simulation of Microwave Antennas without Direct Frequency Scaling," IEEE Proc., vol. 53, No. 6, June 1965, pp. 648-649.

3. Holt, F. Sheppard and Spencer, Roy C., Experimental Optical Investigation of Radar Backscattering, Air Force Cambridge Research Center Report AFCRC-TR-57-106, Antenna Laboratory, 1957.

4. Edison, Allen R., "An Acoustical Model Experiment for Wave Propagation in a Random Medium," IEEE Trans., Sonics and Ultrasonics, vol. SU-11, No. 1, 1964, pp. 30-33.

5. Post, R.E., Guidry, M.R., and Rost, D.F., "A Laboratory Model for Studying Transhorizon Radio Wave Propagation Phenomena," Radio Science J., vol. 3, No. 6, June 1968, pp. 523-527.

6. Hall, Freeman F., Jr., "Temperature and Wind Structure Studies by Acoustic Echo-Sounding," in Seminar and Short Course Report on Remote Sensing of the Troposphere, Chapter 18, V.E. Derr, Ed. Boulder: Bureau of Conference and Institute, University of Colorado, 1972.

7. Little, C. Gordon, "Prospects for Acoustic Echo-Sounding" in Seminar and Short Course Report on Remote Sensing of the Troposphere, Chapter 19, V.E. Derr, Ed. Boulder: Bureau of Conference and Institutes, University of Colorado, 1972.

8. Bean, B.R., "Application of FM-CW Radar and Acoustic Echo-Sounder Technique to Boundary Layer and CAT Studies," in Seminar and Short Course Report on Remote Sensing of the Troposphere, Chapter 20, V.E. Derr, Ed. Boulder: Bureau of Conference and Institutes, University of Colorado, 1972.

9. Kaimal, J.C. and Businger, J.A., "Case Studies of a Convective Plume and a Dust Devil," J. Appl. Meteorol., vol. 9, 1970, pp. 612-620.

10. Du Castel, Francois, Tropospheric Radio Wave Propagation beyond the Horizon. London: Pergamon Press, 1966, pp. 36-38.

11. Friis, H.T., "Microwave Repeater Research," Bell System Technical Journal, vol. 27, No. 2, April 1948, pp. 183-201.

12. Crawford, A.B., and Jakes, W.C., Jr., "Selective Fading of Microwaves," Bell System Technical Journal, vol. 31, No. 1, January 1952, pp. 68-89.

13. Berry, F.A., Bollay, E. and Beers, N.R., Handbook of Meteorology. New York: McGraw-Hill, 1945, pp. 292-295.

14. Riehl, Herbert, Introduction to the Atmosphere, Chapter 3. New York: McGraw-Hill, 1965.

15. Haltiner, George J. and Martin, Frank L., Dynamical and Physical Meteorology, Chapter 6. New York: McGraw-Hill, 1957.

16. Telford, J.W., "The Convection Mechanism in Clear Air," J. of Atmos. Sci., vol. 23, 1966, pp. 652-666.

17. Priestley, C.H.B. and Ball, H.K., "Continuous Convection from an Isolated Source of Heat," Quart. J. Roy. Meteor. Soc., vol. 81, 1955, pp. 144-157.

18. Kuo, H.L., "On the Dynamics of Convective Atmospheric Vortices," J. Atmos. Sci., vol. 23, 1966, pp. 25-42.

19. Huntley, Wright H., Jr., "New Coherent Light Diffraction Techniques," IEEE Spectrum, No. 1, June 1964, pp. 114-122.

20. Bean, B.R. and Dutton, E.J., "Radio Meteorology," National Bureau of Standards Monograph No. 92, 1966, pp. 5-7.

21. Kerr, Donel E., Propagation of Short Radio Waves. New York: Dover, 1965.

22. Wylie, C.R., Jr., Advanced Engineering Mathematics. New York: McGraw-Hill, 1951, pp. 206-208.

23. Liepmann, H.W. and Roshko, A., Element of Gas Dynamics. New York: John Wiley and Sons, 1957, pp. 154-162.

24. Beams, J.W., "Physical Measurements," Chapter 2, in Gas Dynamics and Combustion. Princeton, N.J.: Princeton University Press, 1954, pp. 26-39.

25. Kodak Pamphlet No. P-11, Schlieren Photography, 1960.

26. Waterman, A.T., "A Rapid Beam Swinging Experiment in Transhorizon Propagation," Trans., I.R.E., vol. AP-6, 1958, pp. 338-340.

27. Weinberg, F.J., Optics of the Frame. Washington, D.C.: Butterworth, 1963, pp. 131-132.

28. Selby, S.M., Ed., CRS Standard Mathematical Tables, 16th ed. Cleveland, Ohio: The Chemical Rubber Co., 1968.

IX. ACKNOWLEDGMENT

The author wants to thank the Engineering Research Institute of the Iowa State University for its financial support of this project. He also very much appreciates the help and guidance given to him during his research by his major professor, Dr. Robert E. Post. The author thanks the technicians of the ERI Machine Shop and the ERI Electronics Shop who were very helpful in constructing and fabricating the instruments for this research project.

X. APPENDIX: THEORY OF THE SCHLIEREN SYSTEM

The method for measuring or visualizing the density field of a transparent fluid depends almost entirely on the effects of the fluid density on some form of electromagnetic radiation. These methods may be classified as those which depend on the refractive index (optical method), on absorption, or on emission. Of those, the optical method is by far the best since it does not interfere with the gas being measured [23]. The three principal optical methods are: schlieren, shadowgraph, and interferometer. All depend on the fact that the speed of light varies with the density of the medium through which it passes. The index of refraction n is the ratio of the speed of light in any medium to speed of light in vacuum. Stated mathematically,

$$n = \frac{v_o}{v} \tag{A.1}$$

The refractive index is a function of density for a given substance and a fixed wavelength of light. That is:

$$n = n(\rho) \tag{A.2}$$

To a very good approximation,

$$n = 1 + \beta \frac{\rho}{\rho_s}. \tag{A.3}$$

where ρ_s is the fluid density at standard conditions, and β is a constant for each gas. For air at 0 °C, at pressure of 760 mm. of mercury with light of wavelength 5893 Å, β is equal to 0.000291. The variation of β with wavelength is very small.

The effect of the varying density of the fluid is a verying index of refraction. Light travelling through it will generally follow a curved path. The curvature is in the direction of increasing density. In figure A.1, let the density increase in the positive Y direction. This figure depicts light rays passing through a fluid having a density gradient. The lines marked w_i are the wave fronts and the lines marked r_i, which are orthogonal to the w_i lines, are the ray paths.

Figure A.2 shows the detail of the tilting of the wave fronts. For a small time interval T when the wave front progresses from position w_1 to w_2, we have

$$T = \frac{d\xi}{v} \tag{A.4}$$

where $d\xi$ is the incremental distance in the direction of the ray, v is the speed of the light in the medium, and at (0,0) coordinates. Since the density of the fluid is increasing in the Y direction, the speed of the light is greater along r_1 than along r_2. Let the difference in speeds be dv. The tilting of the wave front will be

$$d\phi = \frac{T|dv|}{d\eta} \tag{A.5}$$

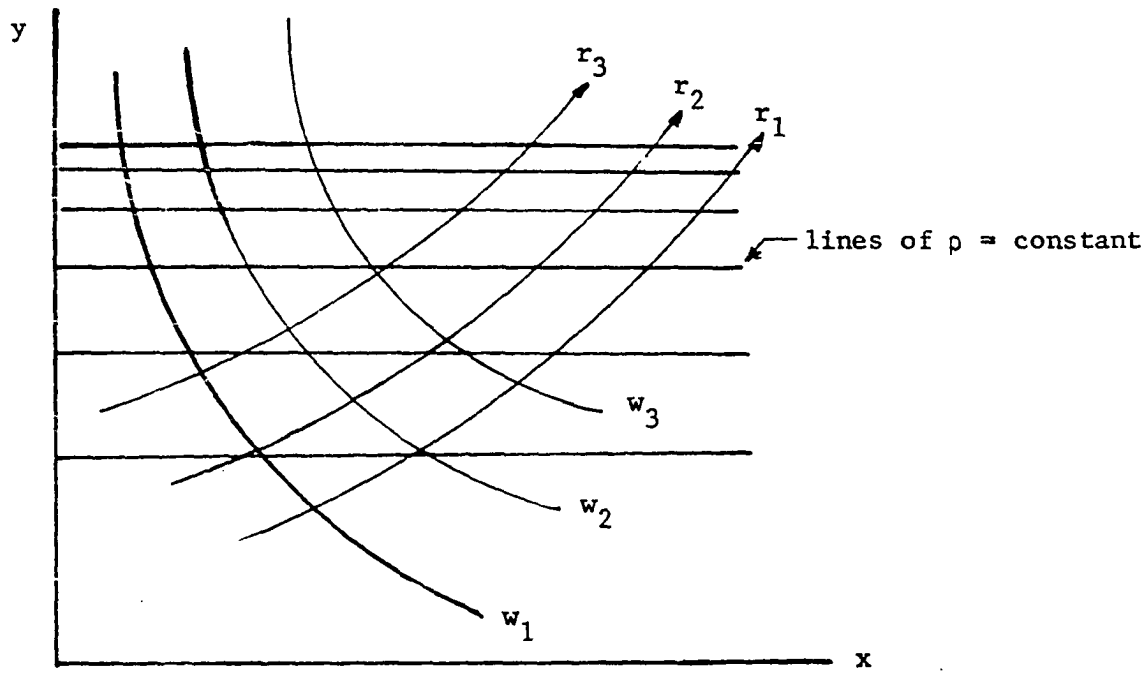

Figure A.1. The light rays passing through a fluid with density gradient in Y direction.

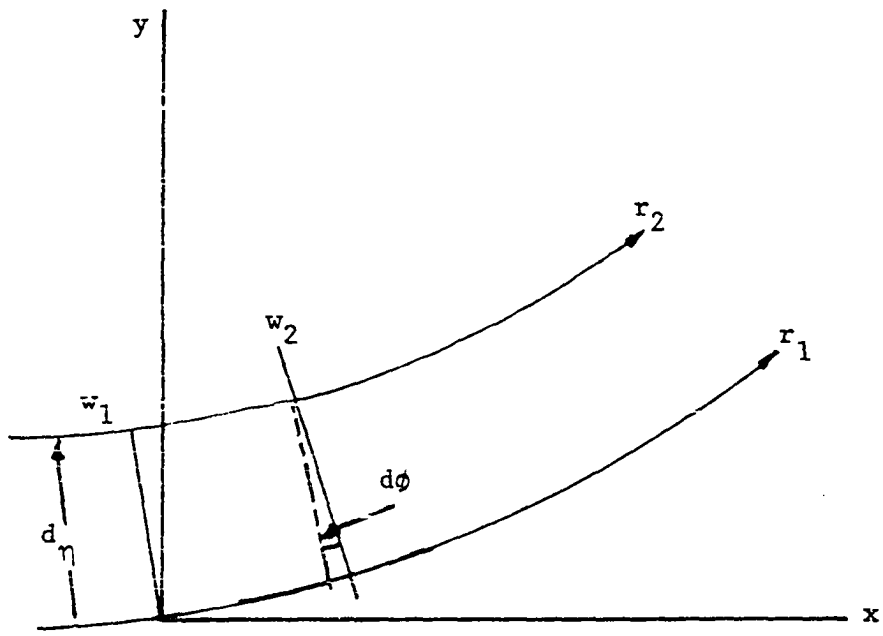

Figure A.2. Details of the tilting of a wave front when the light rays pass through a fluid with density gradient in the Y direction.

where $d\eta$ is the incremental distance in the direction perpendicular to the ray, r_1; and ϕ is the tilting angle.

Since the ray turns through the same angle, the curvature is

$$\frac{1}{R} = \frac{d\phi}{d\xi} \tag{A.6}$$

$$\frac{1}{R} = \frac{1}{v}\frac{|dv|}{|d\eta|} \tag{A.7}$$

$$\frac{1}{R} = \frac{1}{n}\frac{|dn|}{|d\eta|} \, . \tag{A.8}$$

Figure A.3 shows the angular deflection of the ray after it traverses the flow; and, if we let ϵ_y be an angular deflection in the Y direction, then

$$\epsilon_y = \int d\phi \tag{A.9}$$

where the integration is taken along the ray.

For small deflection, the density along the curved ray is nearly the same as along the nearby path, $Y = y_1$. Thus

$$\epsilon_y = \int_0^L \frac{1}{R}\, dx \tag{A.10}$$

$$\epsilon_y = \int_0^L \left(\frac{1}{n}\frac{dn}{dy}\right) \cdot dx \tag{A.11}$$

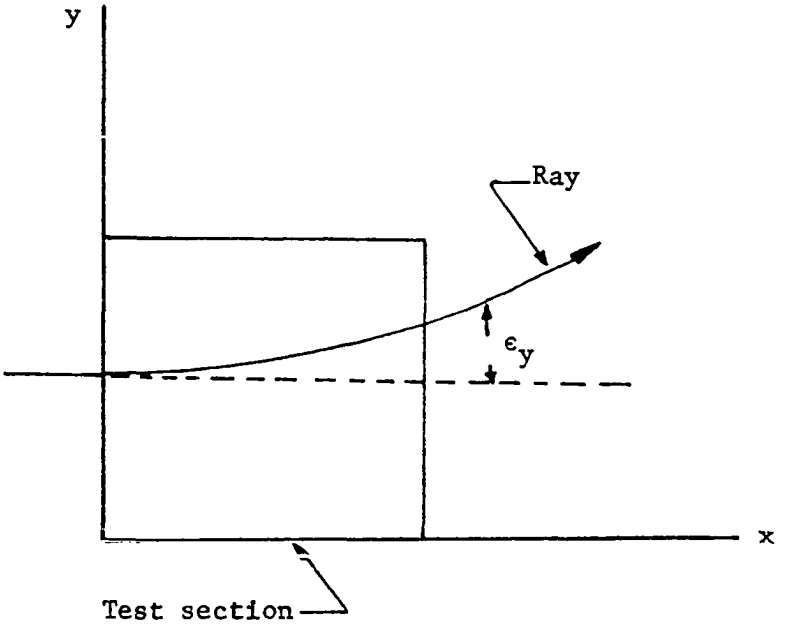

Figure A.3. The deflection of a ray after traversing through the test section.

where L is the length of the test section. The gradient in the Z-direction will cause a curvature of the ray path along the Z-coordinate. For simplicity, we will discuss the Y-component curvature only, since the result can be applied for both directions.

For a plane flow, the integral gives (assuming $n \cong 1$)

$$\epsilon_y = \frac{L}{n} \left(\frac{dn}{dy}\right) \tag{A.12}$$

$$\epsilon_y = \frac{L\beta}{\rho_s} \left(\frac{d\rho}{dy}\right) . \tag{A.13}$$

The above relation shows that, for plane flow, the deflection of the emerging ray is proportional to the density gradient in the fluid.

The basic principle of the schlieren system is to intercept the deflected light, or the undeflected light, before it reaches a viewing screen or the photographic plate, so that part of the source image on the screen becomes darker or brighter. In our case we prefer to block part of the undeflected beam, because our system starts with an unperturbed schlieren field which does not deflect the beam, thus making it easier to adjust the position of the light blocking screen. The opaque screen used to intercept the beam is an ordinary straight edge or knife edge.

Figure A.4 shows one of the possible basic arrangements of the schlieren system [24]. A beam of parallel, monochromatic light is obtained by passing the light source through a lens L_1 and focused on the slit S_1. The light passing S_1 is focused on the knife edge

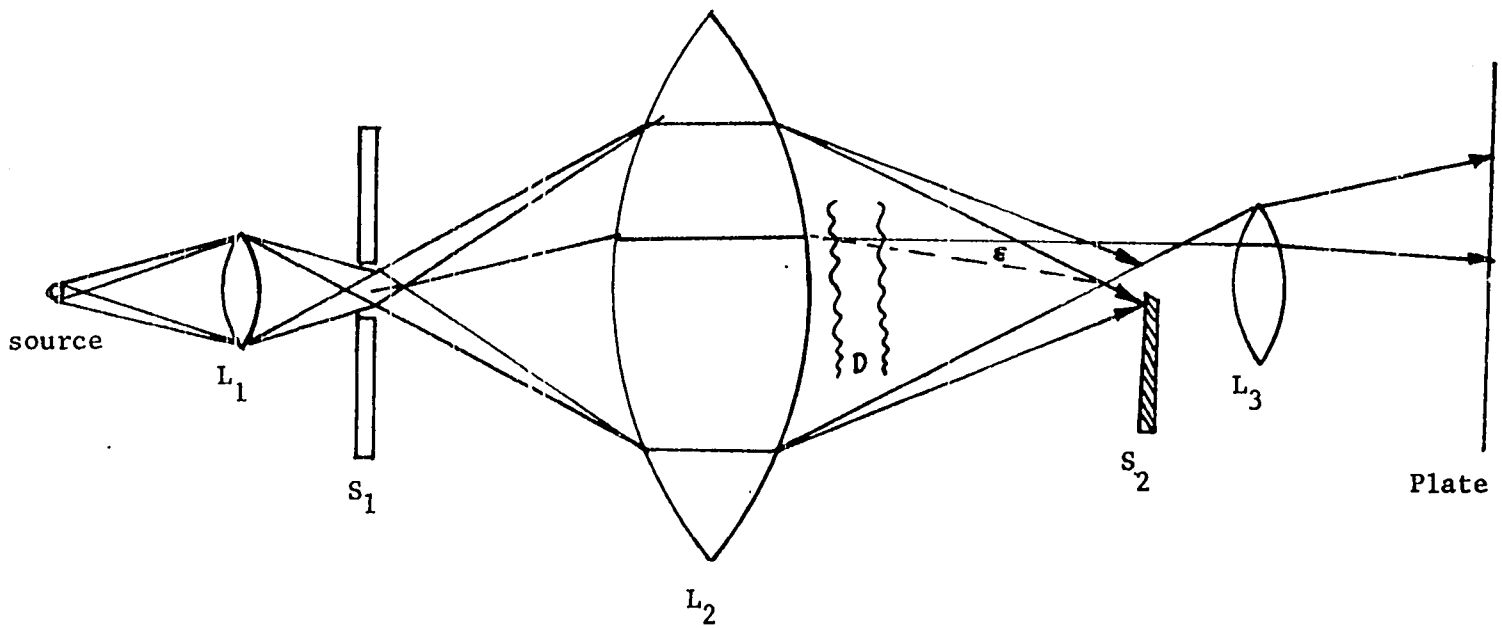

Figure A.4. A basic schlieren system (after J. W. Beams).

S_2, which is in the plane of the image of S_1, by a large diameter lens, called a schlieren lens. The knife edge S_2 is moved into the beam so that only a portion "a" of light beam is left unobstructed. In the absence of a disturbance "D" in the beam, each point of the photographic plate "p" received uniform illumination intensity "I", which proportional to the width "a" of the light beam allowed to pass by the knife edge S_2. Once the disturbance is introduced, the deflection suffered by the rays will induce a shift in the source image formed by this light in the plane of S_2. The intensity of illumination at the corresponding point on the photographic plate will now have changed by an amount "ΔI" which is proportional to the component of the shift "Δa" normal to the knife edge. Thus, the contrast on the viewing screen will relate to the deflection of rays as [25]

$$\frac{\Delta I}{I} = \frac{\Delta a}{a} \quad . \tag{A.14}$$

By geometrical optics Δa is equal to $f_2 \tan\epsilon$, where f_2 is the focal length of the second lens of figure A.4.

At the viewing screen the local relative brightness or contrast becomes a function of x and y [23],

$$\frac{\Delta I}{I} = C(x,y) = \frac{f_2 \tan\epsilon}{a} \quad . \tag{A.15}$$

By the assumption that we are dealing with a planar flow, the increase or decrease of illumination at the screen is proportional to

the density gradient in the flow. Thus, if we replace the screen with a photographic plate and take a picture of the illuminated flow, we can estimate the gradient of the fluid in the flow.

The arrangement of the schlieren system using lenses as shown in figure A.4 requires high quality, large diameter, long focal-length lenses [27]. The lenses used must be free of chromatic and spherical aberrations. The large diameter is required because the cross section of the disturbance can be large, and the long focal length is necessary in order to get the requisite precision and image size.

In experiments requiring that large regions of disturbance be investigated, the necessarily large, high quality lenses become quite expensive. So the concave mirror has been used in experiments of this type. The high optical quality, long focal length and large diameter requirements can be met by a mirror system with much less expense.

Figure A.5 shows the arrangement of a schlieren system using two concave mirrors. These mirrors should be grounded to a surface accuracy of better than one tenth of a wavelength of the source. The source is placed at the focal plane of the first mirror while the two mirrors are separated by a distance suitable for the encompassing of the region of turbulence. The knife edge is positioned in the focal plane of the second mirror.

From equations (A.13) and (A.15), the fractional change of the illumination of the screen is given by

$$\frac{\Delta I}{I} = \frac{f_2}{a} \tan \left(\frac{L\beta}{\rho_s}\left(\frac{\partial \rho}{\partial y}\right)\right) \qquad \text{(A.16)}$$

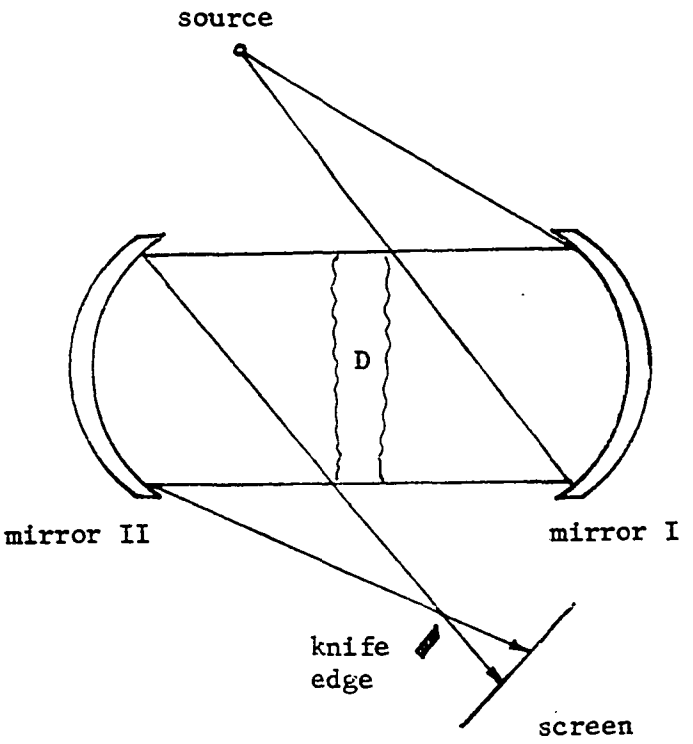

Figure A.5. The two mirrors schlieren system arrangement.

The light increase is then captured on a photographic plate and the plate then processed with time and temperature control such that the density of negative is a linear function of the intensity of light. Then the refractive index gradients can be calculated [24].

In case of nonplanar flow, such as the flow of air in the boundary of the thermal plume the behavior of the flow can be observed as outlined in the following analysis. Assume that the hot air column is cylindrical in shape with a circular cross section and having a homogeneous medium inside the boundary whose refractive index is less than that of the air surrounding it. Let the radius of the plume be R and i and r be the angles of incidence and refraction respectively.

Consider one of the rays incident on the surface of the plume. Since the refractive index of air inside the plume is less than that of the air outside, the ray will be deviated upward as shown in figure A.6. Applying Snell's law we have

$$\frac{\sin i}{\sin r} = {}_{c}n_{h} \tag{A.17}$$

where ${}_{c}n_{h}$ is the refractive index of air inside (hot) with respect to the air outside (cold). Let ϵ be the angular deviation from the original ray direction, then we have

$$\epsilon = 2(r - i) \tag{A.18}$$

and

$$i = \sin^{-1}(h/R) \tag{A.19}$$

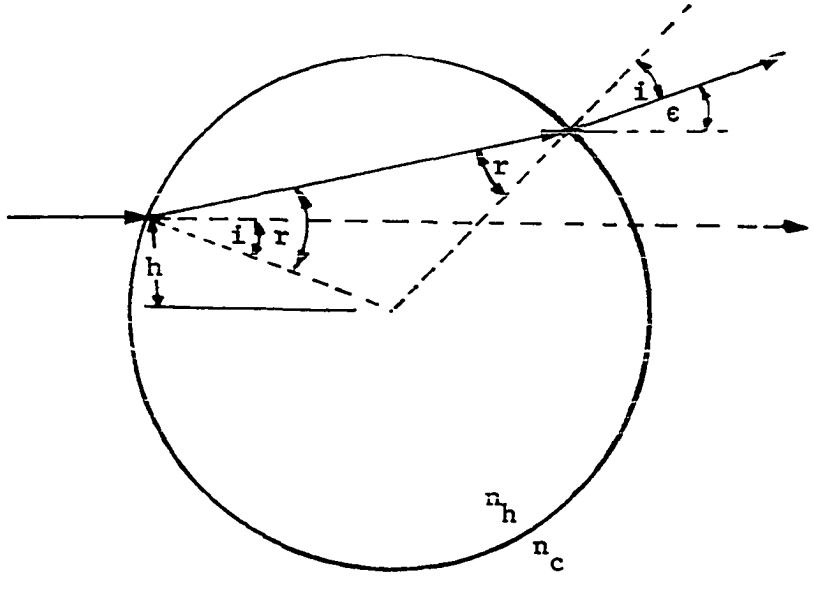

Figure A.6. The geometrical optic of a light ray passing through the thermal plume.

where h is the distance from the center of the boundary to the point where the ray strikes the surface. Substituting into Equation (A.18) we have

$$\epsilon = 2(\sin^{-1} \frac{h}{{}_{c}n_{h} R} - \sin^{-1} \frac{h}{R}) \qquad (A.20)$$

As h decreases, the angles become small, then

$$\epsilon \cong 2(\frac{h}{R}) [\frac{1}{{}_{c}n_{R}} - 1] \qquad (A.21)$$

From the above equation, (A.21), we see that ϵ is proportional to the distance h as h tends to be zero. That is the light rays seem to emerge from the same point as h approaches zero. For points far from the axis, h/R approaches unity, and $h/{}_{c}n_{h}R > 1$. From equation (A.20), term $\sin^{-1} h/{}_{c}n_{h}R$ has its last real value, that is $\pi/2$ when $h = R \times {}_{c}n_{h}$. For $h > R \times {}_{c}n_{h}$, ϵ becomes imaginary. This means that the rays will be reflected when they strike the boundary surface.

If this hot air column were put in the test section of the schlieren system and a knife edge used to block some part of the beam, the relative increasing of light or contrast on the screen is

$$\frac{\Delta I}{I} = \frac{f_2}{a} \tan[2(\sin^{-1} h/{}_{c}n_{h} \cdot R) - \sin^{-1}(h/R)] \qquad (A.22)$$

where h is less than R but still large. When h approaches zero the relative light increase becomes

$$\frac{\Delta I}{I} = \frac{f_2}{a} \tan[2(h/R)(1/{}_c n_h - 1)] \qquad (A.23)$$

where ΔI is the change in illumination, I is the illumination when there is no deviation, f_2 is the focal length of the second mirror, a is the portion of light that passes through the screen, ${}_c n_h$ is the refractive index of hot air with respect to the surrounding air.

From equations (A.22) and (A.23) we can see that the term f_2/a is a constant for each knife edge position; thus, it is called a sensitivity factor which defined as the fractional increase (or decrease) of light deflection obtained at the knife edge for unit angular deflection of the ray at the test section. Its value varies inversely with the amount of light passed (or blocked).

In figure A.7, which shows the curve of relative brightness at the screen, the Y-axis represents the value of h, and the X-axis represents the value of light illumination on the screen with the origin corresponding to the center of the column. At center and close to it where h is small, the illumination is I since fewer light rays are deviated away from their original path. When the value of h increased, the relative light change $\Delta I/I$ becomes tangent function (equation (A.23)). The approximation of $\sin\theta = \theta$ fails when θ is about 0.1 degree [28], or when $h/R = .00175$. Then, when h reaches value of .00175R the relative change in illumination $\Delta I/I$ becomes a more complicated function. Since the deviation of a light ray from any point in the schlieren field corresponds to a change

in illumination by the source of that point on the screen, every point of the image of the source on the screen will have a relative brightness of

$$\frac{I-\Delta I}{I} = \frac{f_2}{a} - \frac{f_2}{a}\tan\left[2\left(\frac{h}{R}\right)(1/n_h - 1)\right] \qquad \text{(A.24)}$$

$$= \frac{f_2}{a} - \frac{f_2}{a}\tan\left[2\left(\sin^{-1}\frac{h}{n_h \cdot R} - \sin^{-1}\frac{h}{R}\right)\right] \qquad \text{(A.25)}$$

A curve representing the relative brightness on the screen for the case of a column of heated air in the schlieren field is shown in figure A.7.

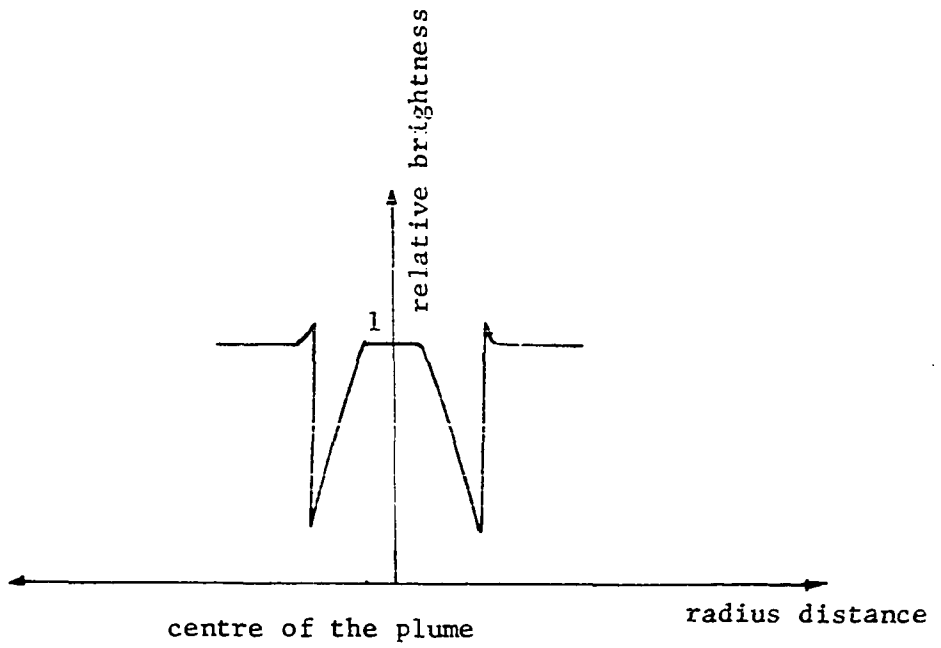

Figure A.7. The relative brightness on the screen due to the deflection of light after passing through a hot air column.